General Disclaimer

One or more of the Following Statements may affect this Document

- This document has been reproduced from the best copy furnished by the organizational source. It is being released in the interest of making available as much information as possible.

- This document may contain data, which exceeds the sheet parameters. It was furnished in this condition by the organizational source and is the best copy available.

- This document may contain tone-on-tone or color graphs, charts and/or pictures, which have been reproduced in black and white.

- This document is paginated as submitted by the original source.

- Portions of this document are not fully legible due to the historical nature of some of the material. However, it is the best reproduction available from the original submission.

NASA TECHNICAL MEMORANDUM

NASA TM X- 71940

NASA TM X-71940

PATTERNS OF BROAD-BEAM ANTENNAS OF DIFFERENT POLARIZATIONS NEXT TO SIMPLE HANGAR MODELS

by C. R. Cockrell

April 1977

NASA
National Aeronautics and Space Administration

Langley Research Center
Hampton, Virginia 23665

1. Report No. NASA TM X-71940	2. Government Accession No.	3. Recipient's Catalog No.

4. Title and Subtitle	5. Report Date
PATTERNS OF BROAD-BEAM ANTENNAS OF DIFFERENT POLARIZATIONS NEXT TO SIMPLE HANGAR MODELS	April 13, 1977
	6. Performing Organization Code
7. Author(s)	8. Performing Organization Report No.
C. R. Cockrell	
	10. Work Unit No. 505-07-41-01
9. Performing Organization Name and Address	11. Contract or Grant No.
NASA Langley Research Center Hampton, Virginia 23665	
	13. Type of Report and Period Covered
12. Sponsoring Agency Name and Address	Technical Memorandum
National Aeronautics and Space Administration Washington, D. C. 20546	14. Sponsoring Agency Code

15. Supplementary Notes

16. Abstract

Broad-beam antennas of different polarizations radiating next to simple hangar models are investigated. Expressions that represent the elevation-plane patterns of slots in and 1/4 λ monopoles on a finite rectangular ground plane upon which a rectangular scattering object has been placed have been derived using geometrical theory of diffraction. These expressions were obtained by superposing the infinite ground plane solutions, reflected field solutions from the scattering object and diffracted field solutions in their respective regions of validity. Patterns for a 1/2 λ slot (two orientations) and 1/4 λ electric monopole are verified experimentally for a number of source locations. Data pertaining to the polarization question in regard to the multipath problem are presented.

17. Key Words (Suggested by Author(s))	18. Distribution Statement
Broad-beam antennas, Diffraction, Multipath, Horizontal and Vertical Polarizations	Unclassified - Unlimited STAR Category 07

19. Security Classif. (of this report)	20. Security Classif. (of this page)	21. No. of Pages	22. Price*
Unclassified	Unclassified	39	$4.00

*For sale by the National Technical Information Service, Springfield, Virginia 22161

PATTERNS OF BROAD-BEAM ANTENNAS OF DIFFERENT POLARIZATIONS NEXT TO SIMPLE HANGAR MODELS

By C. R. Cockrell

SUMMARY

Broad-beam antennas of different polarizations radiating next to simple hangar models are investigated. Expressions that represent the elevation-plane patterns of slots in and 1/4 λ monopoles on a finite rectangular ground plane upon which a rectangular scattering object has been placed have been derived using geometrical theory of diffraction. These expressions were obtained by superposing the infinite ground plane solutions, reflected field solutions from the scattering object, and diffracted field solutions in their respective regions of validity. Patterns for a 1/2 λ slot (two orientations) and 1/4 λ electric monopole are verified experimentally for a number of source locations. Data pertaining to the polarization question in regard to the multipath problem are presented.

INTRODUCTION

Whenever an aircraft approaches runways near an air terminal, the antenna onboard may receive signals from a ground antenna via many paths: (1) direct radiation, (2) reflected radiation from the ground and any obstacle that may reflect electromagnetic energy to either antenna, and (3) diffracted radiation which results from edges and curved obstacles. This many-path problem has been given the terminology "multipath" (refs. 1, 2). Since reflected and diffracted signals can have adverse effects on landing systems, knowledge of the strength and location of these signals is of great interest. Once this

information has been obtained, modifications to the trouble-causing obstacles (such as hangars) could be implemented. Possibly, the use of corrugated surfaces on buildings and hangars could be used to reduce the effect of scattered energy (refs. 2, 3). This paper, however, is not concerned with what can be done to reduce or eliminate the interfering signals but is concerned primarily with overall effects of the scattering obstacles on the total signal.

The obstacles around air terminals may be very complex structures and, therefore, greatly complicate the analysis of predicting the total radiation pattern of an antenna located in their vicinity. To formulate a mathematical model which completely describes such a complex problem would be a monumental task. One approach to the problem, however, would be to model less complicated obstacles and then build from these solutions to the more complex solutions. A practical problem would be one of broad-beam antennas radiating near hangars; measurements of such patterns are not available for comparison with theoretical analysis.

In this paper, the radiation fields of a slot and a monopole in a finite ground plane upon which a scattering object is mounted are analyzed via geometrical theory of diffraction (GTD) (ref. 4). The analysis consists of supplementing the radiation fields for the slot and monopole in an infinite ground plane by the additional field contributions arising from the reflection off the scattering object and diffraction by the edges of the object and by the edges of the finite ground plane. By allowing the edge to be moved farther from the scattering object, the practical problem mentioned in the previous paragraph can be better approached.

The infinite ground plane solutions are readily obtained using either aperture integration or Fourier transform techniques over an assumed aperture

field distribution for slot antennas and the vector potential technique for a monopole above an infinite ground plane. These resulting fields may be viewed as the fields associated with rays directly radiated by the aperture (monopole) in (on) the infinite ground plane. These infinite ground plane solutions are then only valid in regions which are not blocked by any scattering object on the ground plane and above the ground plane itself.

The resultant fields thus far formulated are modified by including the reflections from the flat face of the object placed on the ground plane and by employing the compact dyadic edge diffraction coefficient developed by Kouyoumjian and Pathak (ref. 4) at the ground plane and object edges. Their edge diffraction coefficient provides a field which is discontinuous in such a manner as to compensate for the discontinuities associated with the incident and reflected fields so that the total field is continuous throughout. The diffracted field, therefore, supplements the infinite ground plane field and reflected field in their range of validity and accounts solely for the field in the shadow region (behind the scattering object and behind the ground plane) where the infinite ground plane field and reflected field are zero.

To verify the analysis, scale models on finite ground planes were built. Elevation-plane patterns for two different scattering objects placed on a finite ground plane were measured for five different source locations. The type sources used were the electric quarter-wavelength monopole and the half-wavelength narrow rectangular slot (both orientations to simulate both polarizations). These measured patterns were compared to the computed patterns obtained by using the expressions derived in this paper. Calculated patterns for the magnetic quarter-wavelength monopole source are included to further investigate the question of polarization.

THEORY

A. Infinite Ground Plane Solutions

The infinite ground plane solutions are the far field solutions for a slot (a by b) within an infinite perfectly conducting ground plane and for a 1/4 λ monopole on an infinite perfectly conducting ground plane. These solutions are readily obtained by Fourier transform techniques or aperture integration techniques. The aperture distributions within (on) the slot (monopole) are assumed to be sinusoidal along their lengths and uniform in their transverse directions. With reference to figure 1, the far-field expressions for the case when the narrow dimension (a) of the rectangular slot is parallel to the face of the scattering object are given as

$$\left.\begin{aligned} E^s_{\theta\perp} &\sim \cos\phi\ \hat{F}_x\ \frac{e^{-jkr}}{r} \\ E^s_{\phi\perp} &\sim \sin\phi\cos\theta\ \hat{F}_x\ \frac{e^{-jkr}}{r} \\ H^s_{\phi\perp} &= 1/Z_0\ E^s_{\theta\perp} \\ H^s_{\theta\perp} &= -\,1/Z_0\ E^s_{\phi\perp} \end{aligned}\right\} \qquad (1)$$

where

$$\hat{F}_x = \frac{\sin\left(\frac{ka}{2}\sin\theta\cos\phi\right)}{\frac{ka}{2}\sin\theta\cos\phi}\ \frac{\cos\left(\frac{kb}{2}\sin\theta\sin\phi\right) - \cos\frac{kb}{2}}{k^2 - (k\sin\theta\sin\phi)^2} \qquad (2)$$

Similarly, the far-field expressions when the long dimension (a) of the slot is parallel to the face of the scattering object are given as

$$
\begin{aligned}
E^s_{\theta\parallel} &\sim \sin\phi\ \hat{F}_y \frac{e^{-jkr}}{r} \\
E^s_{\phi\parallel} &\sim \cos\phi\ \cos\theta\ \hat{F}_y \frac{e^{-jkr}}{r} \\
H^s_{\phi\parallel} &= 1/Z_0\ E^s_{\theta\parallel} \\
H^s_{\theta\parallel} &= -1/Z_0\ E^s_{\phi\parallel}
\end{aligned}
\tag{3}
$$

where

$$
\hat{F}_y = \frac{\sin\left(\frac{kb}{2}\sin\theta\sin\phi\right)}{\frac{kb}{2}\sin\theta\sin\phi}\ \frac{\cos\left(\frac{ka}{2}\sin\theta\cos\phi\right) - \cos\frac{ka}{2}}{k^2 - (k\sin\theta\cos\phi)^2} \tag{4}
$$

The far-field expressions for electric and magnetic quater-wavelength monopoles on a infinite ground plane are given, respectively, as

$$
\left.
\begin{aligned}
E^m_{\theta\parallel} &\sim \frac{\cos\left(\frac{\pi}{2}\cos\theta\right)}{\sin\theta}\ \frac{e^{-jkr}}{r} \\
H^m_{\phi\parallel} &\sim \frac{1}{Z_0}\ \frac{\cos\left(\frac{\pi}{2}\cos\theta\right)}{\sin\theta}\ \frac{e^{-jkr}}{r}
\end{aligned}
\right\} \tag{5}
$$

and

$$\left.\begin{aligned} H^{m}_{\theta\perp} &\sim \frac{\cos\left(\frac{\pi}{2}\cos\theta\right)}{\sin\theta}\,\frac{e^{-jkr}}{r} \\ E^{m}_{\phi\perp} &\sim -Z_0\,\frac{\cos\left(\frac{\pi}{2}\cos\theta\right)}{\sin\theta}\,\frac{e^{-jkr}}{r} \end{aligned}\right\} \tag{6}$$

By restricting the analysis to the y-z plane ($\phi = 90, 270$), the field components perpendicular to the y-z plane for equations (1), (3), (5) and (6) are written, respectively, as

$$E^{is}_{x\perp} \sim \cos\theta\left[\frac{\cos\left(\frac{kb}{2}\sin\theta\right) - \cos\frac{kb}{2}}{k^2 - (k\sin\theta)^2}\right]\frac{e^{-jkr}}{r} \tag{7}$$

$$H^{is}_{x\parallel} \sim \frac{1}{Z_0}\left[\frac{\sin\left(\frac{kb}{2}\sin\theta\right)}{\frac{kb}{2}\sin\theta}\left(\frac{1 - \cos\frac{ka}{2}}{k^2}\right)\right]\frac{e^{-jkr}}{r} \tag{8}$$

$$H^{im}_{x\parallel} \sim \frac{1}{Z_0}\left[\frac{\cos\left(\frac{\pi}{2}\cos\theta\right)}{\sin\theta}\right]\frac{e^{-jkr}}{r} \tag{9}$$

$$E^{im}_{x\perp} \sim -Z_0\left[\frac{\cos\left(\frac{\pi}{2}\cos\theta\right)}{\sin\theta}\right]\frac{e^{-jkr}}{r} \tag{10}$$

where

$$k = \omega(\mu_0\varepsilon_0)^{1/2}$$

$$Z_0 = (\mu_0/\varepsilon_0)^{1/2} \tag{11}$$

B. Reflected Fields From Vertical Structure

Image theory is employed to determine the fields from the vertical reflecting surface shown in figure 1; i.e., the reflected fields are the fields produced by "imaged sources" which are placed an equidistance behind the reflecting surface as the real sources are placed in front. The strength, phase and polarization of these fields depend on the strength, phase and polarization of the real sources at the reflecting points. These reflected fields are only valid in the range of real source angles which intercept the reflecting surface. For a typical reflection point, the components of the reflected fields corresponding to the components of the direct fields given in equations (7-10) are given, respectively, as

$$E_{x\perp}^{rs} \sim -\cos\theta_i \left[\frac{\cos\left(\frac{kb}{2}\sin\theta_i\right) - \cos\frac{kb}{2}}{k^2 - (k\sin\theta_i)^2}\right]\frac{e^{-jkR}}{R} \tag{12}$$

$$H_{x\parallel}^{rs} \sim \frac{1}{Z_0}\left[\frac{\sin\left(\frac{kb}{2}\sin\theta_i\right)}{\frac{kb}{2}\sin\theta_i}\left(\frac{1 - \cos\frac{ka}{2}}{k^2}\right)\right]\frac{e^{-jkR}}{R} \tag{13}$$

$$H_{x\parallel}^{rm} \sim \frac{1}{Z_0}\left[\frac{\cos\left(\frac{\pi}{2}\cos\theta_i\right)}{\sin\theta_i}\right]\frac{e^{-jkR}}{R} \tag{14}$$

$$E_{x\perp}^{rm} \sim Z_0\left[\frac{\cos\left(\frac{\pi}{2}\cos\theta_i\right)}{\sin\theta_i}\right]\frac{e^{-jkR}}{R} \tag{15}$$

where θ_i is incident angle of the source field at the reflecting surface and R is the distance from the image source to the field point.

C. Diffracted Fields From Ground Plane Edge and Vertical Structure Edge

A detailed description of electromagnetic wedge diffraction is given in reference 4. Applications, based on the diffraction coefficients derived in reference 4, are given in reference 5.

From reference 4 the diffracted electric and magnetic fields may be expressed, respectively, as

$$\underline{E}^d \sim \underline{E}^i (Q_E) \cdot \overline{\overline{D}}_E \left[\frac{s'}{s(s' + s)}\right]^{1/2} e^{-jks}$$

$$\underline{H}^d \sim \underline{H}^i (Q_E) \cdot \overline{\overline{D}}_H \left[\frac{s'}{s(s' + s)}\right]^{1/2} e^{-jks} \qquad (16)$$

where $\underline{E}^i (Q_E)$ and $\underline{H}^i (Q_E)$ are the electric and magnetic fields, respectively, at a point Q_E on the edge (on the ground plane or any edge of vertical structure) which is incident from the source (or an edge which acts like a source) and $\overline{\overline{D}}_{E,H} = - \hat{\beta}_0\hat{\beta}_0 D_h - \hat{\phi}'\hat{\phi} D_s$. The distances s' and s and the unit vectors are shown in figure 2a. $D_{s,h}$ is given by (ref. 4, eq. 113 or ref. 5, eq. 4)

$$D_{s,h} = \frac{1}{\sin\beta_0}\left[\left\{d^+(\beta^-,n)F\left[Ka^+(\beta^-)\right] + d^-(\beta^-,n)F\left[Ka^-(\beta^-)\right]\right\}_+^- \left\{d^+(\beta^+,n)F\left[Ka^+(\beta^+)\right]\right.\right.$$

$$\left.\left. + d^-(\beta^+,n)F\left[Ka^-(\beta^+)\right]\right\}\right] \qquad (17)$$

where (ref. 4, eq. 114 or ref. 5, eq. 5)

$$d^{\pm}(\beta,n) = \frac{\exp(-j\pi/4)}{n(2\pi k)^{1/2}} \frac{1}{2} \cot \frac{\pi \pm \beta}{2n} \quad \text{in which} \quad \beta = \beta^{\pm} = \phi \pm \phi' \qquad (18)$$

and (ref. 4, eq. 115 or ref. 5, eq. 6)

$$F\left[Ka^{\pm}(\beta)\right] = 2_j\left|\left[Ka^{\pm}(\beta)\right]^{1/2}\right|\exp\left[jKa^{\pm}(\beta)\right]\int_{\left[Ka^{\pm}(\beta)\right]^{1/2}}^{\infty}\exp\left(-j\tau^2\right)d\tau \tag{19}$$

where (ref. 4, eq. 116 or ref. 5, eq. 7)

$$a^{\pm}(\beta) = 1 + \cos\left(-\beta + 2n\,N^{\pm}\pi\right) \tag{20}$$

in which $N^{\pm}$ is the positive or negative integer or zero, which most nearly satisfies (ref. 4, eq. 117 or ref. 5, eq. 8)

$$\begin{aligned} 2n\pi N^{-} - \beta &= -\pi \\ 2n\pi N^{+} - \beta &= \pi \end{aligned} \tag{21}$$

$K = kL$ where k = free-space wavenumber and $L = \dfrac{s's\sin^2\beta_0}{s + s'}$.

The diffracted field problem for the 2-dimensional geometry shown in figure 2-b is now formulated for the different type sources considered in this paper. Since the application in mind is one of an aircraft or helicopter in the vicinity of buildings, hangars, etc., the analysis is further restricted to the coverage above the ground plane shown in figure 1. Diffracted fields from the points A, B, C, and D are included in the analyses. The diffracted fields or rays from A-P and B-P are the direct-diffracted rays which are valid so long as they are not blocked by a scattering object (ground plane and vertical structure). The rays C-P and D-P are referred to as the diffracted-diffracted rays which depend on the strength of the fields at A and B, respectively. The rays A-Q-P and B-Q'-P are diffracted-reflected rays. Each of the rays discussed has its range of validity and care must be exercised in

whether a particular ray should be included in the total field. Many additional multiple diffractions could be included but for the geometries considered in this paper their contributions to the total field are small and therefore have been omitted. Rather than explicitly writing the diffracted field for every case discussed above, it will merely be stated that the contribution from each of the diffraction points can be written in the form indicated by equations (16). A superposition of the complex diffracted fields, the direct fields and the reflected fields make up the total field.

CALCULATED AND MEASURED RESULTS

The model consisted of a 1.27 × 30.48 × 60.96 cm aluminum ground plane in which five square holes were cut. The distances between the holes were chosen arbitrarily but unequal to allow for more general source locations. Only one hole at a time was used for the slot or monopole source, hence, the remaining four holes were plugged so that continuity in the ground plane at these holes was maintained. Aluminum rectangular scattering objects were placed on the ground plane 7.62 cm (8.89 λ) from the closest hole (source).

Elevation-plane patterns for two rectangular scattering objects 5.08 × 6.35 cm (5.92 λ × 7.41 λ) and 7.62 × 6.35 cm (8.89 λ × 7.41 λ) and for two type sources (1/2 λ slot and 1/4 λ electric monopole) were measured; the measurements were made for the five different source locations at a frequency of 35 GHz. To investigate both parallel and perpendicular polarizations on the scattering object, both slot orientations were included in the measurements.

For comparison calculated elevation-plane patterns, using the analysis described in this paper, and measured elevation-plane patterns are shown in

figures 3-6. Figures 3 and 4 are the patterns for the 1/2 λ slot with h = 5.08 cm (5.92 λ) and h = 7.62 cm (8.89 λ) scattering objects, respectively, and figures 5 and 6 are the patterns for the 1/4 λ electric monopole with the same two scattering objects. The agreement obtained in these patterns is quite good, even in the detail of the ripple in the patterns; thereby, demonstrating that the equations developed in this paper do predict the patterns quite well (see figs. 3-6). The greatest disagreement occurs in the region of least interest which is behind the scattering object; the agreement in this region could be improved if diffractions from the back edge of the ground plane were included in the analysis. The magnitude of the ripple in the patterns decreases as the source distance increases; this is easily seen in the parallel-polarization patterns shown in figures 3 and 4.

To gain further insight into the polarization question, calculated patterns for a magnetic monopole were performed for the same five locations as the electric monopole. Figure 8 compares the magnitude of the ratios, direct/indirect fields, of the electric and magnetic monopole sources at the five different locations for h = 5.08 cm (5.92 λ) scattering object as a function of the elevation-plane angle, θ. Inspection of these figures clearly shows that both parallel and perpendicular-polarized antennas can produce indirect fields (reflected and diffracted fields) which can be greater than the direct field. The greater indirect fields for parallel polarization, however, occur for a wider range of angles. In fact, indirect fields greater than the direct field do not occur at all for perpendicular polarization for magnetic monopoles located 19.05 cm (22.22 λ) and 25.40 cm (29.63 λ) away from the scattering object (see figures 8d and 8e). Computer runs on more realistic physical models were made, resulting in essentially the same

conclusions; i.e., that indirect fields can be greater than direct fields but with more rapid variations in the total field off the ground plane edge. It should be pointed out that any conclusions as to which polarization is best for a system can critically depend on the particular system application and geometry of the problem.

CONCLUDING REMARKS

Expressions that represent the elevation-plane patterns of slots in and 1/4 λ monopoles on a finite rectangular ground upon which a rectangular scattering object has been place have been derived using geometrical theory of diffraction. The agreement between the measured and calculated elevation-plane patterns is quite good for both slot and monopole sources. This agreement demonstrates that the analysis developed in this paper is a valid one and suggests the possibility of using the same techniques for more complex problems. The results of the simple models investigated do offer invaluable information about the polarization question; i.e., polarization selection in regards to multipath depends on the application and the geometry of the problem.

REFERENCES

1. RTC "A New Guidance System for Approach and Landing" SC117 Document No. DO-148, December 18, 1970.

2. Brindley, A. E., et. al, Multipath Environment Evaluation, IIT Research Institute, Tech. Report AFFDL-TR-74-150, November 1974.

3. Brindley, A. E., et. al, A Joint Army/Air Force Investigation of Reflection Coefficients at C and Ku Bands for Vertical, Horizantal and Circular System Polarizations, IIT Research Institute, Tech. Report AFFDL-TR-76-67, July 1976.

4. Pathak, P. H. and Kouyoumjian, R. G., "The Dyadic Diffraction Coefficient for a Perfectly Conducting Wedge," Electro Science Lab., Ohio State University, Columbus, Rep. 2183-4, June 5, 1970, Contract No. AF19 (628)-5929.

5. Cockrell, C. R. and Pathak, Prabhakar H., "Diffraction Theory Techniques Applied to Aperture Antennas on Finite Circular and Square Ground Planes," IEEE Trans. on Antennas and Propagation, Vol. AP-22, No. 3, May 1974.

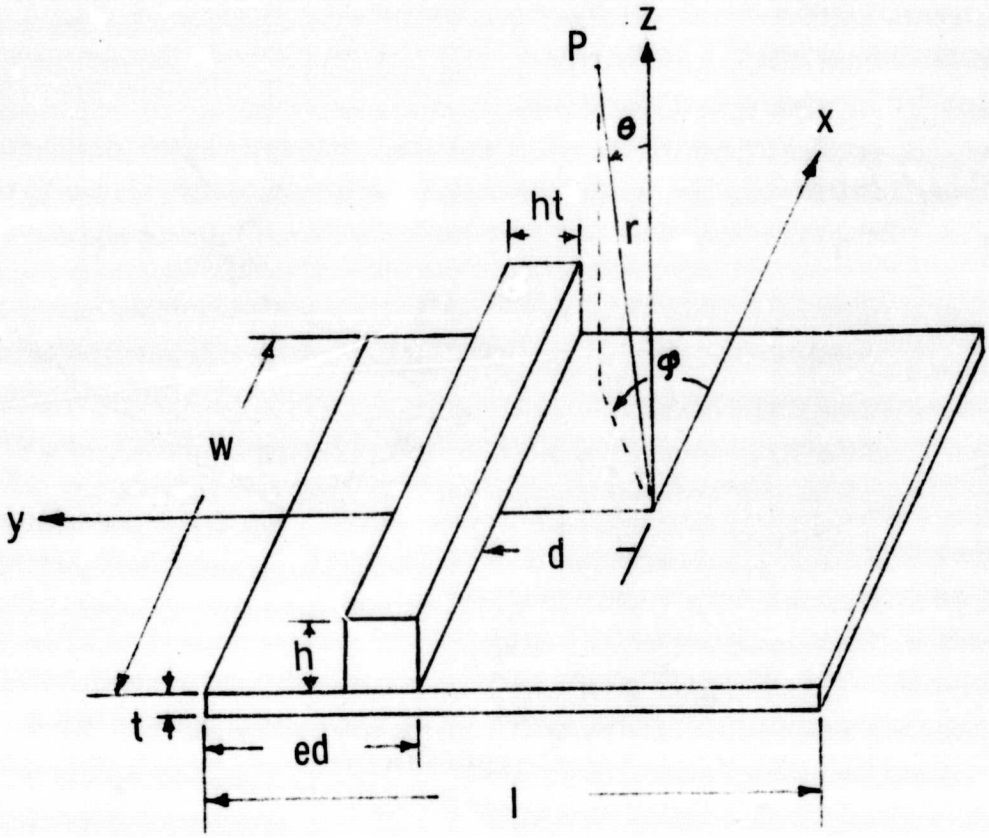

	dimension in cm.	dimension in wavelengths
t	1.27	1.48
ht	6.35	7.41
ed	17.78	20.74
w	30.48	35.56
l	60.96	71.12

Fig. 1. Model of geometry.

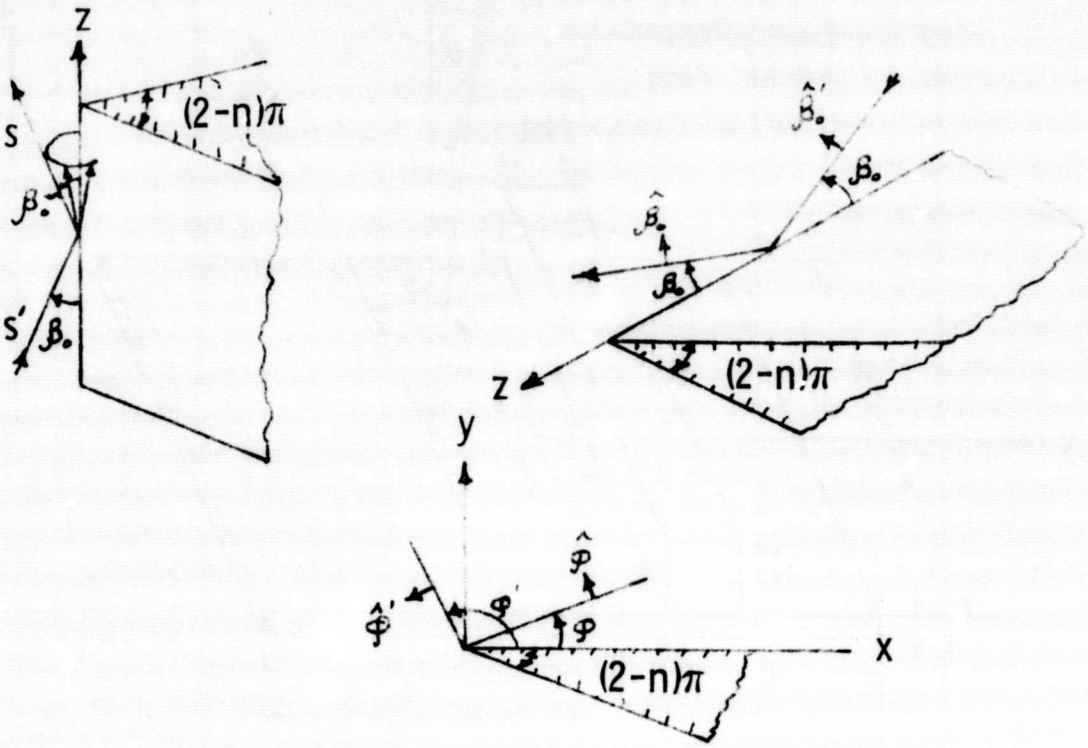

a) general rays

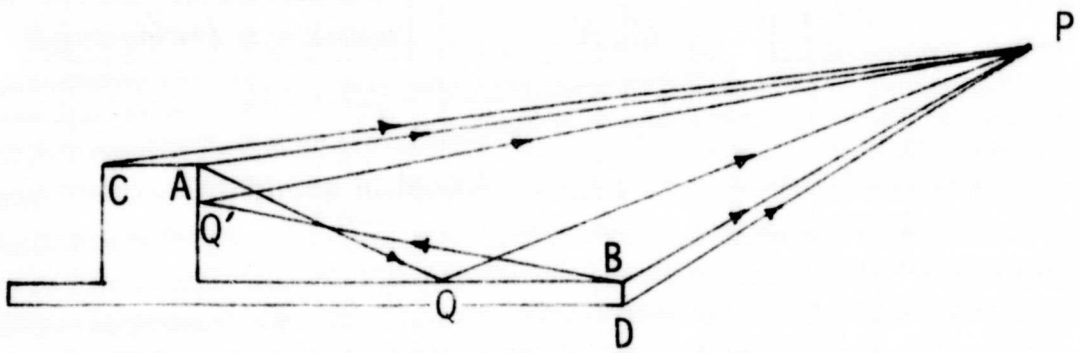

b) rays for two-dimensional geometry of Fig. 1.

Fig. 2. Geometry for diffracted rays.

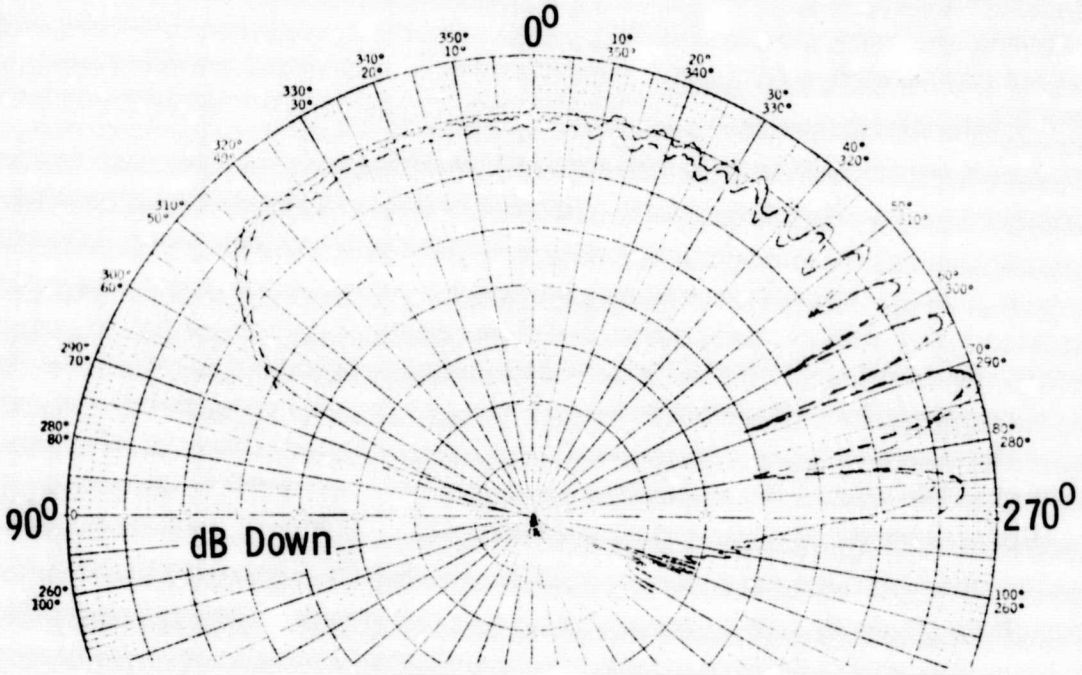

parallel polarization

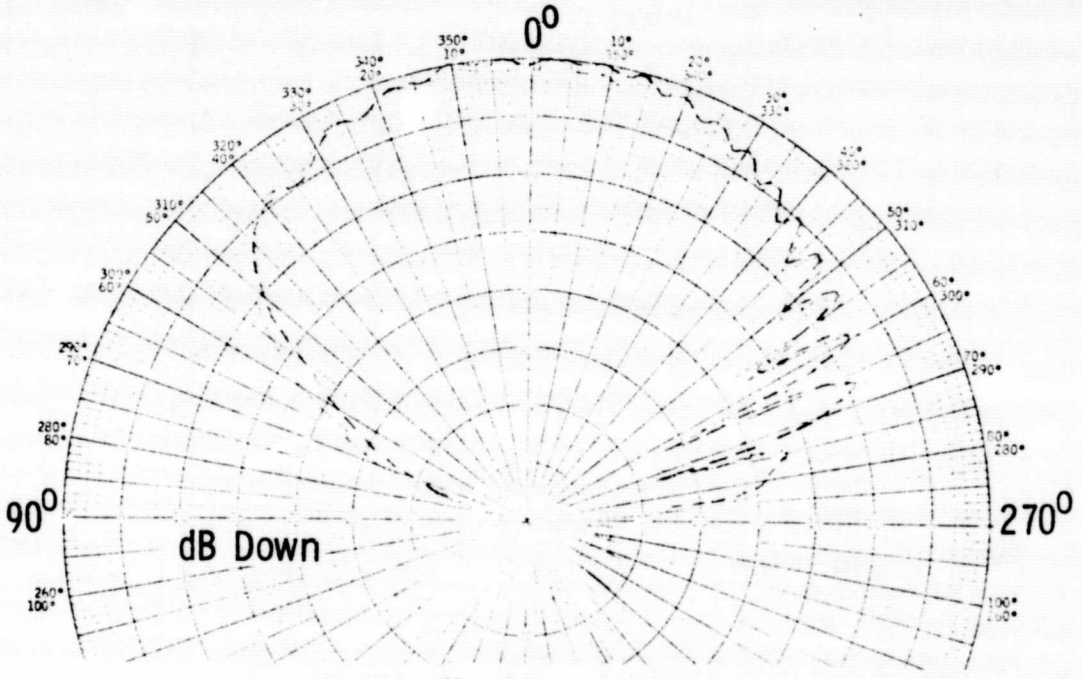

perpendicular polarization

a) d=7.62 cm

Fig. 3. Elevation-plane patterns of $1/2\lambda$ slot for h= 5.08 cm at 35. GHz. Calculated– – –, Measured———.

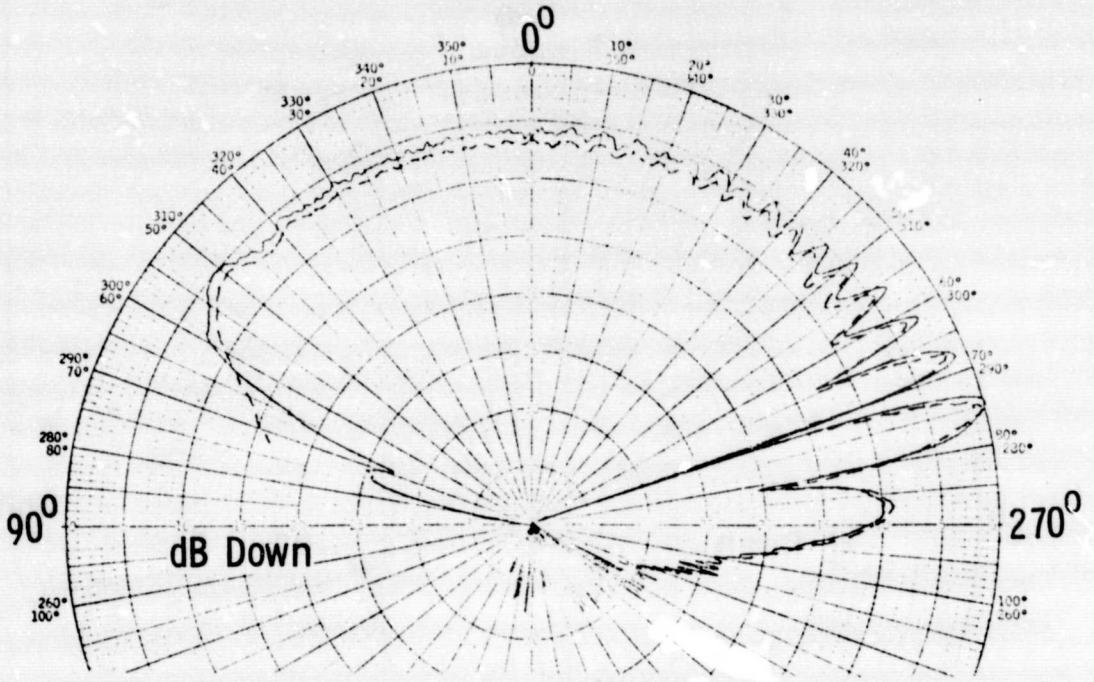

parallel polarization

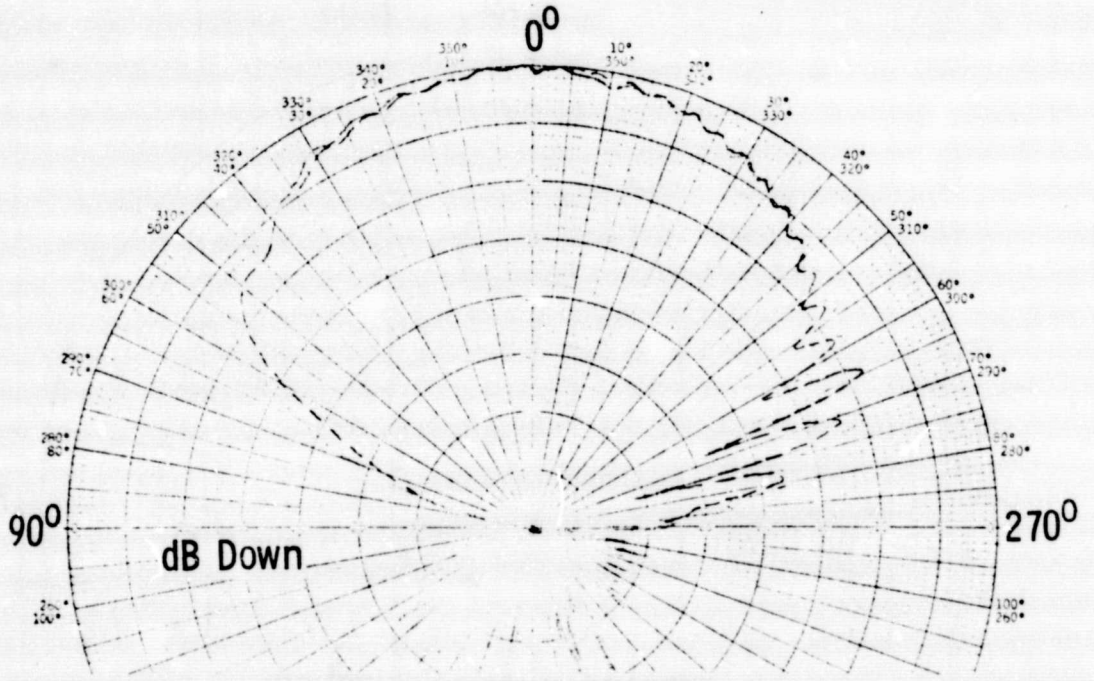

perpendicular polarization

b) d=10.16 cm

Fig. 3. Continued.

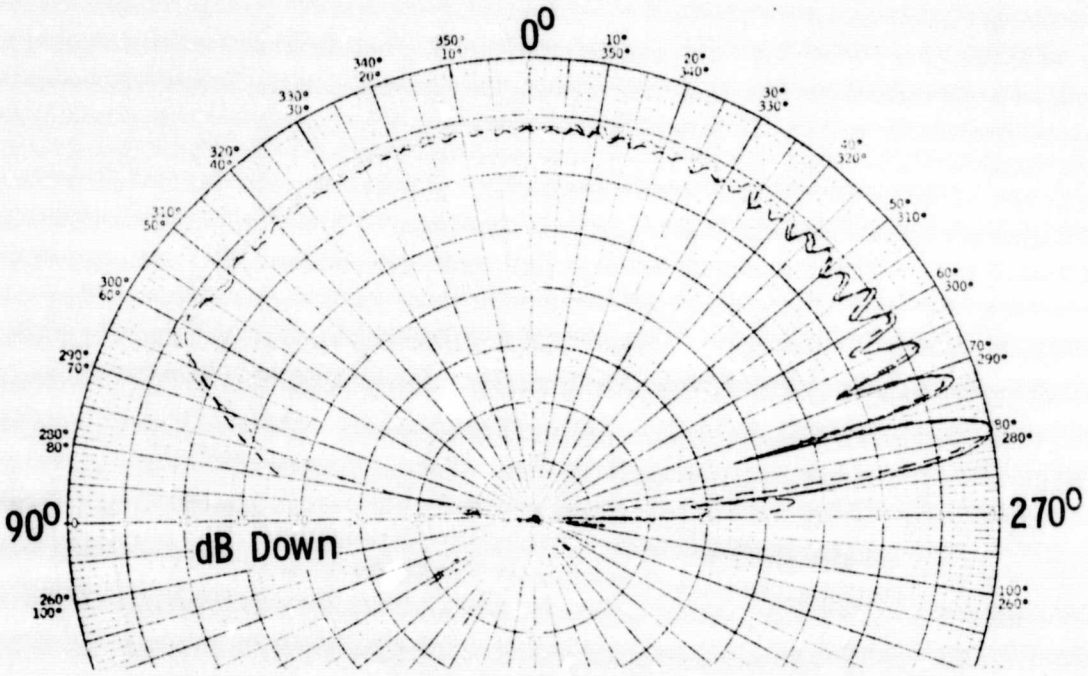

parallel polarization

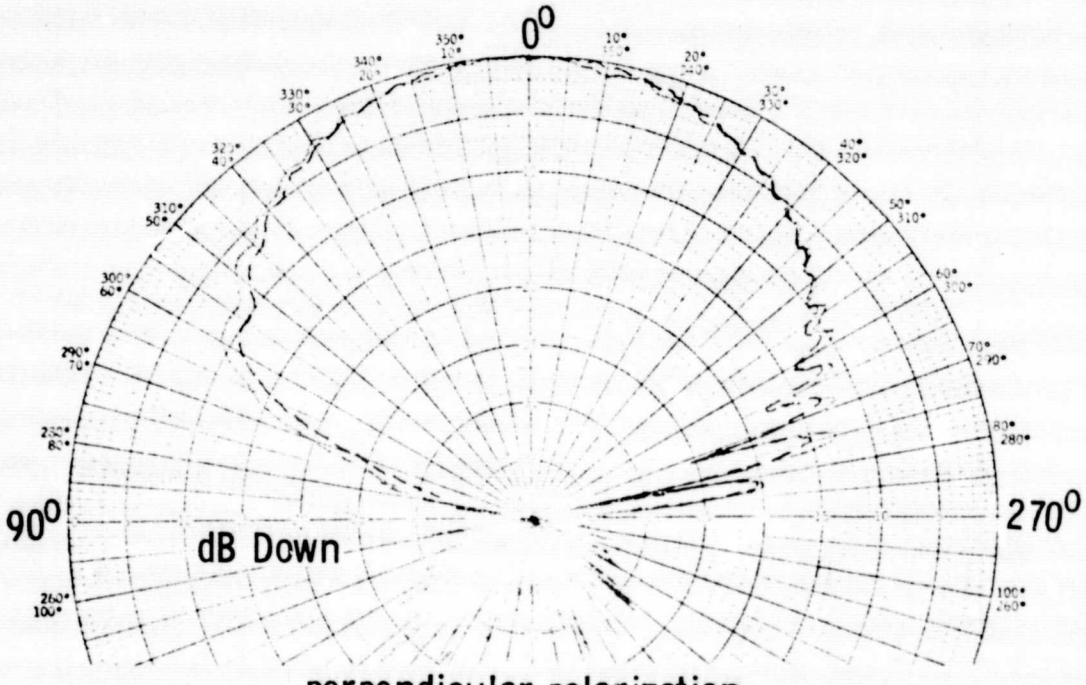

perpendicular polarization

c) d = 13.94 cm

Fig. 3. Continued.

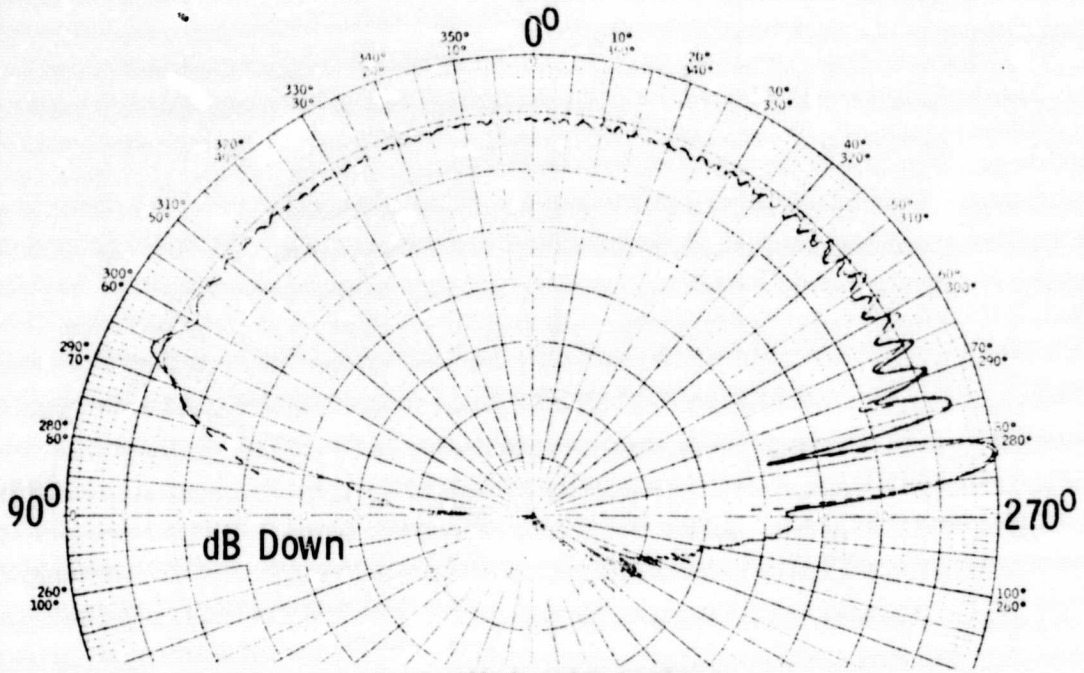

parallel polarization

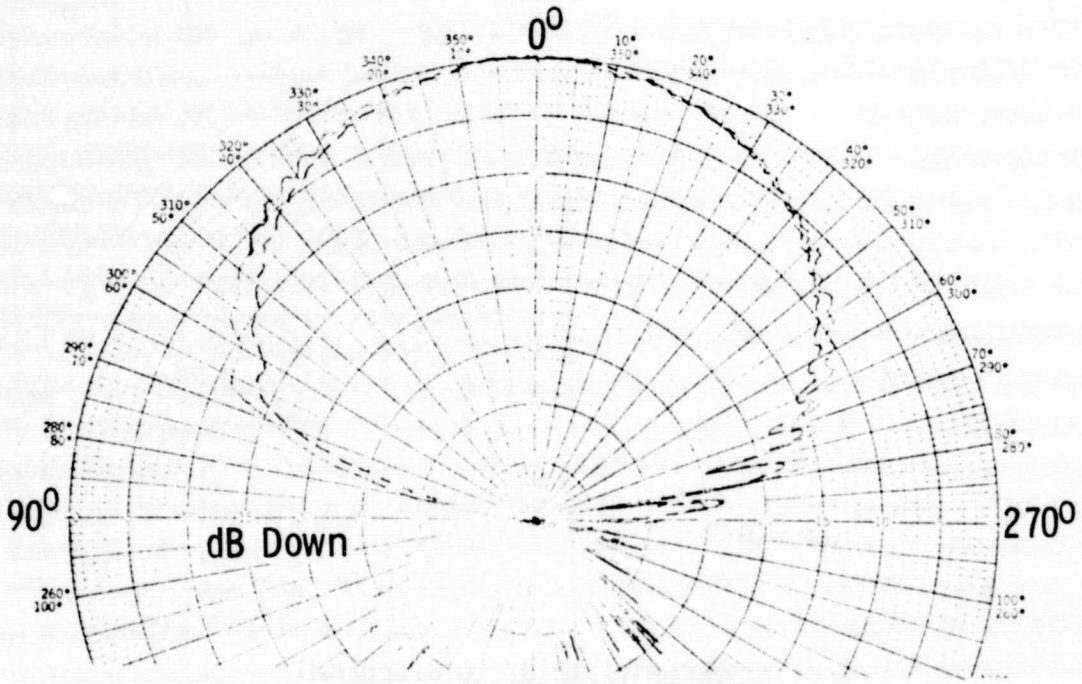

perpendicular polarization

d) d = 19.05 cm

Fig. 3. Continued.

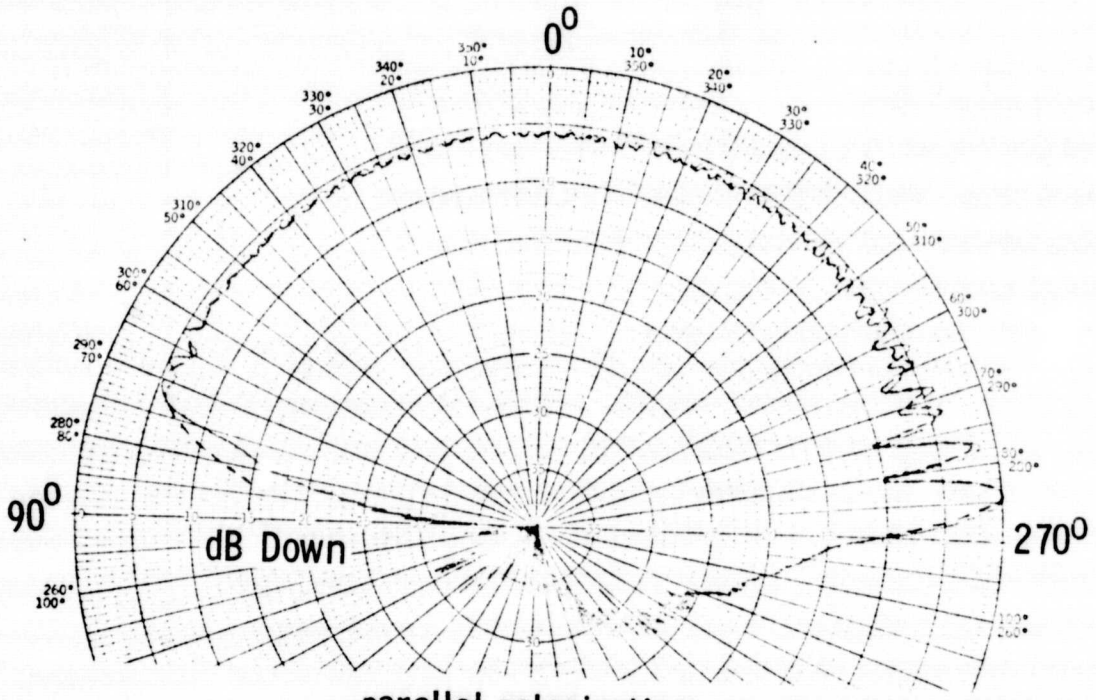

parallel polarization

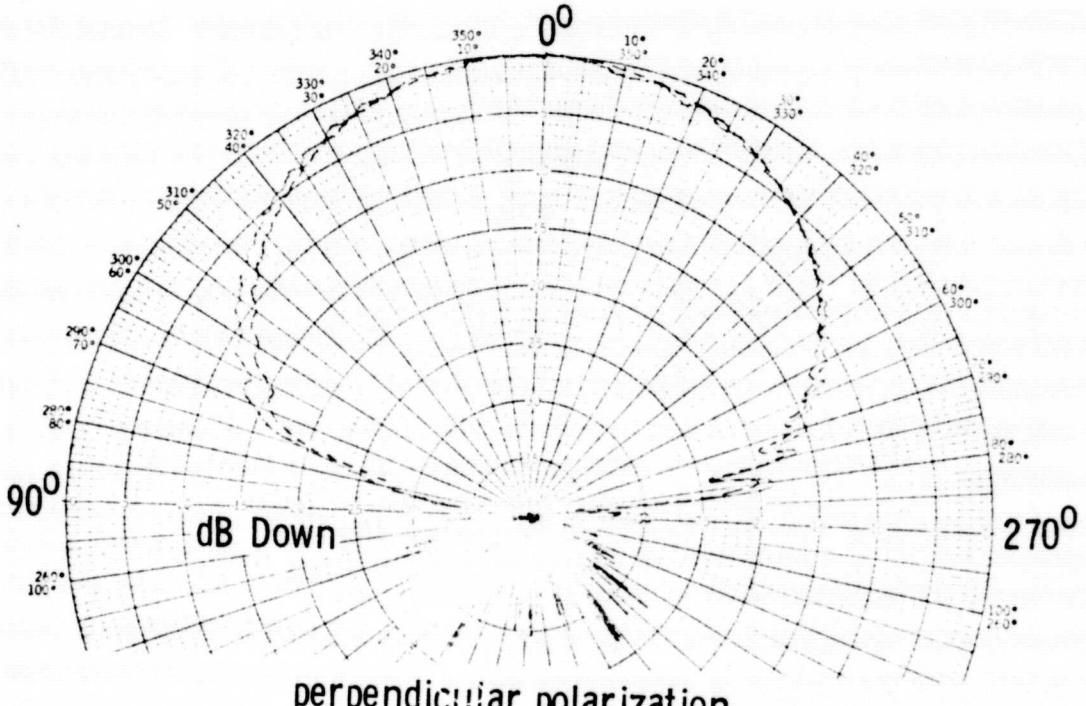

perpendicular polarization

e) d = 25.40 cm

Fig. 3. Concluded.

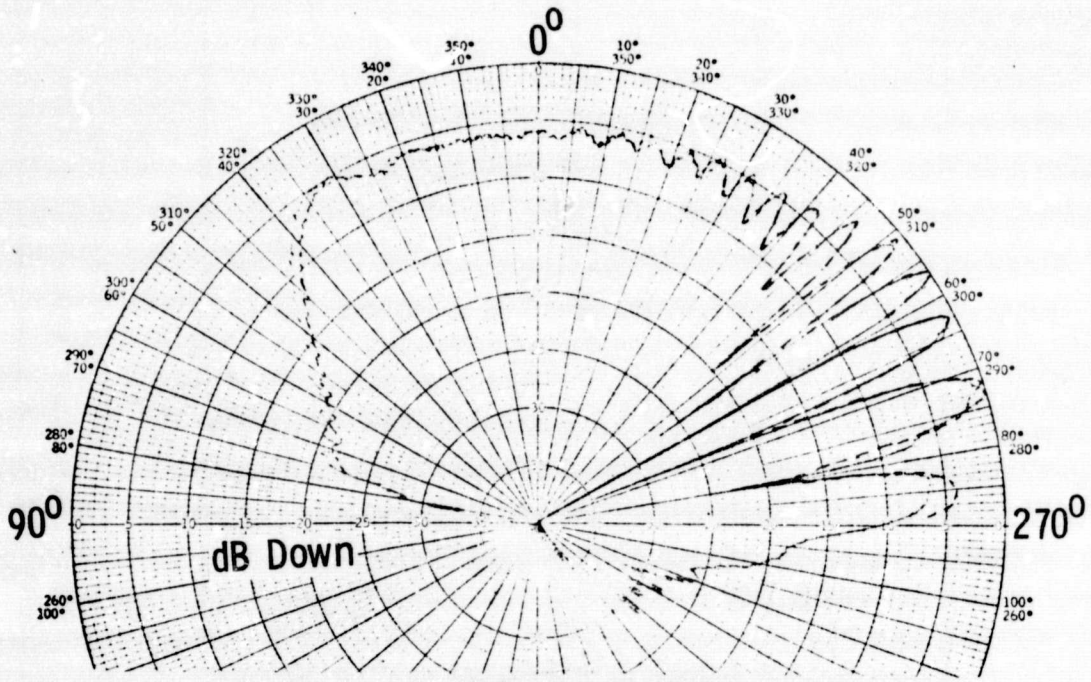

parallel polarization

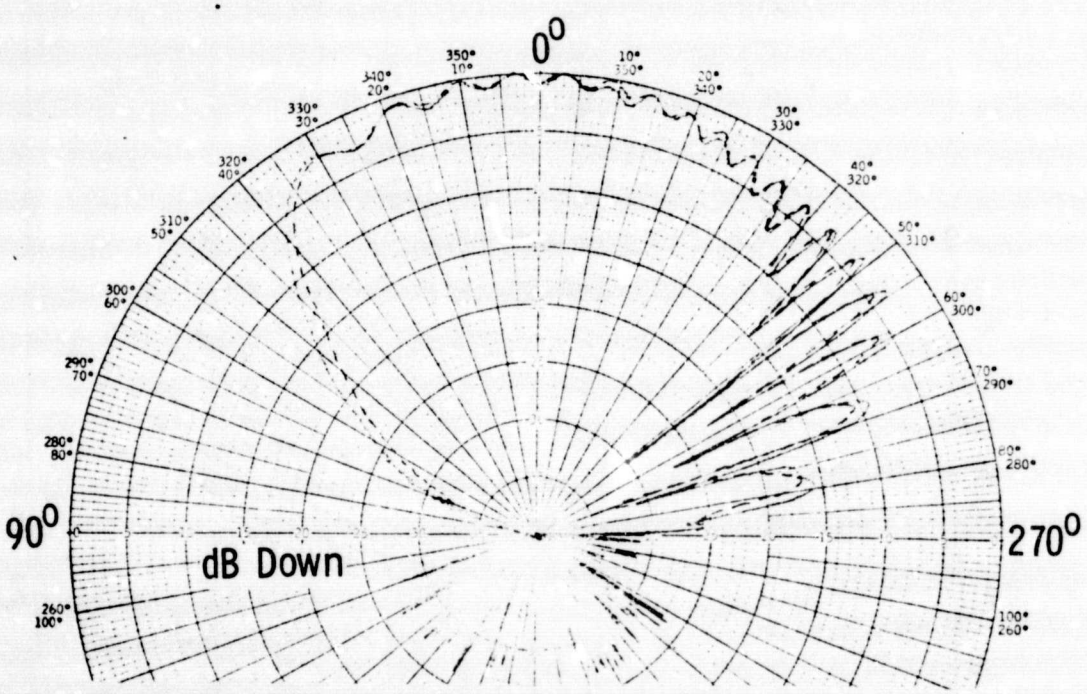

perpendicular polarization

a) d = 7.62 cm

Fig. 4. Elevation-plane patterns of $1/2\lambda$ slot for h = 7.62 cm at 35. GHz. Calculated – – –, Measured ——— .

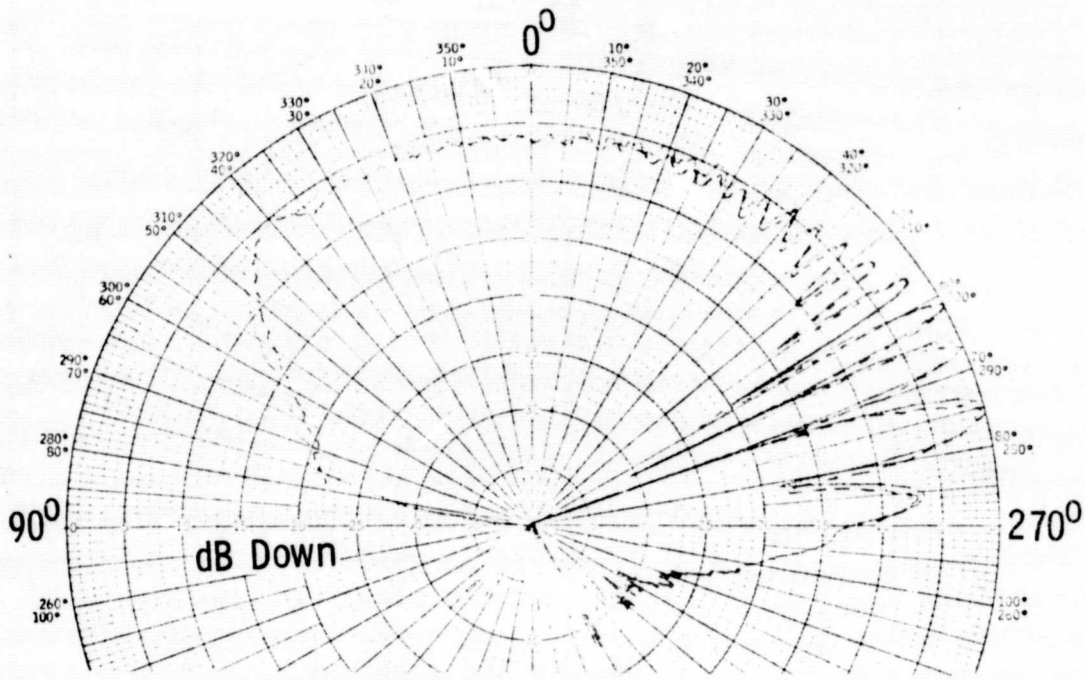

parallel polarization

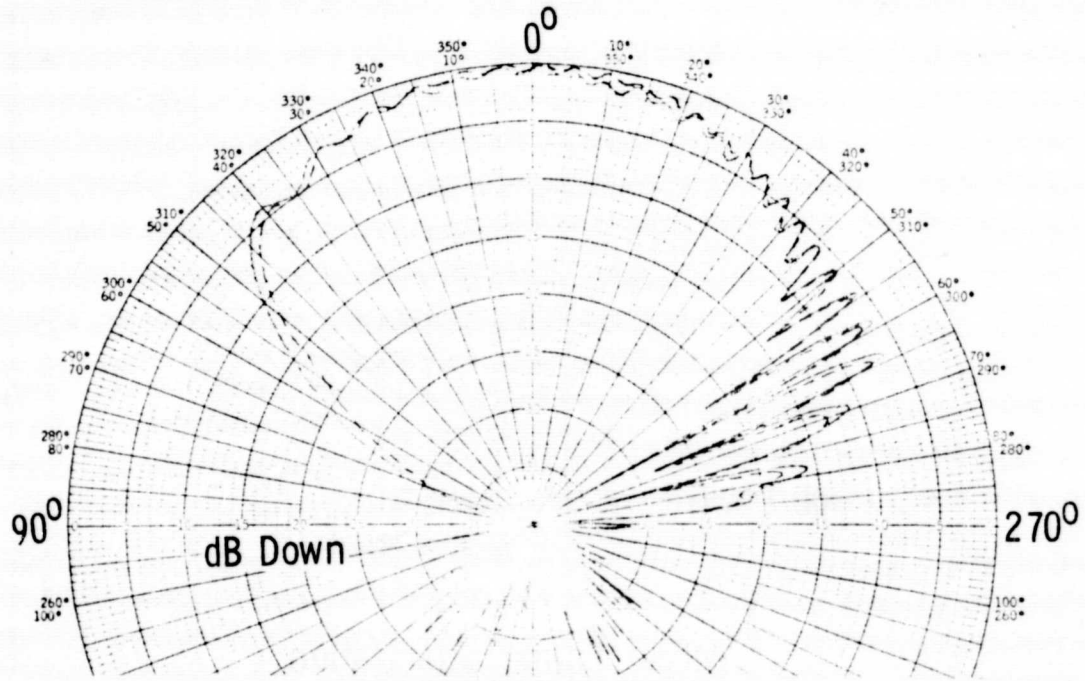

perpendicular polarization

b) d=10.16 cm

Fig. 4. Continued.

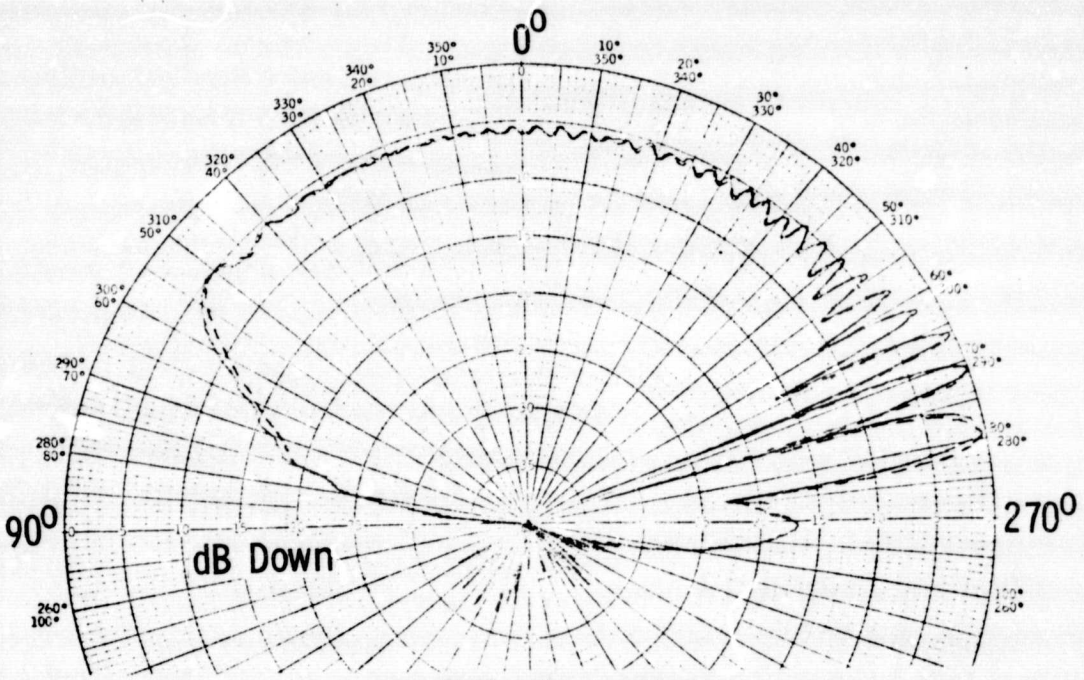

parallel polarization

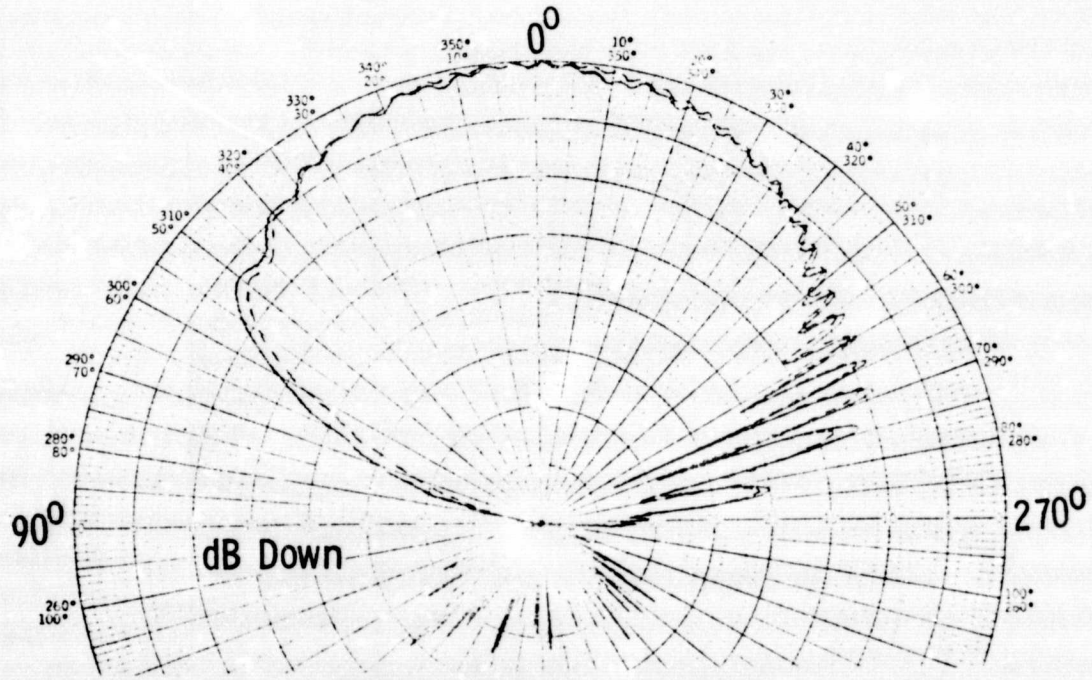

perpendicular polarization

c) d = 13.94 cm

Fig. 4. Continued.

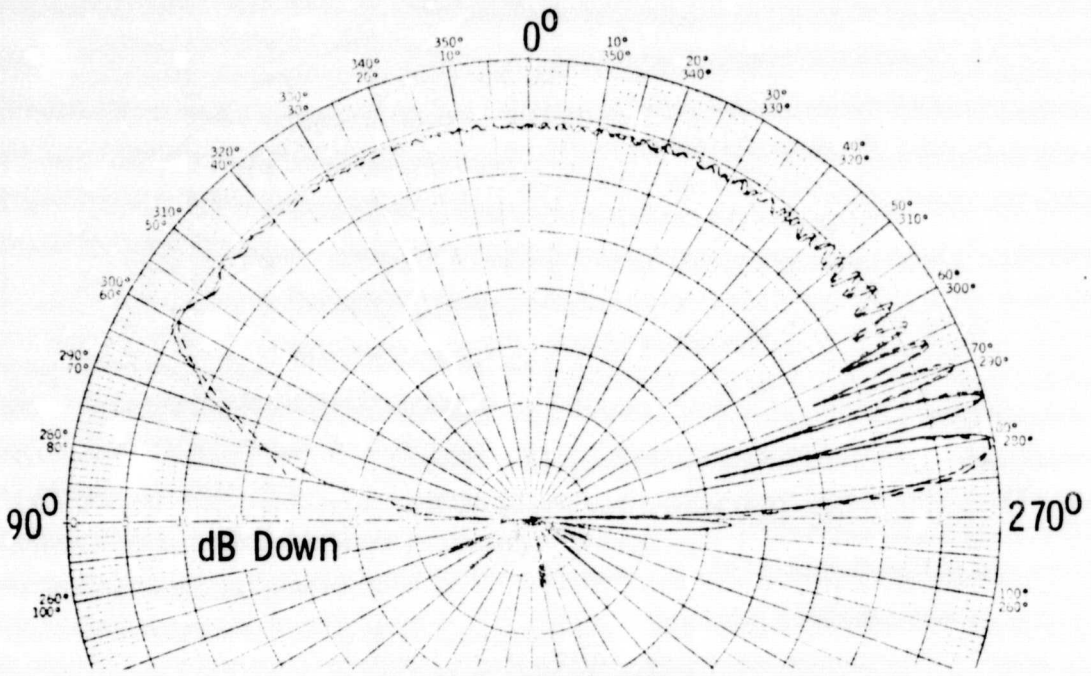

parallel polarization

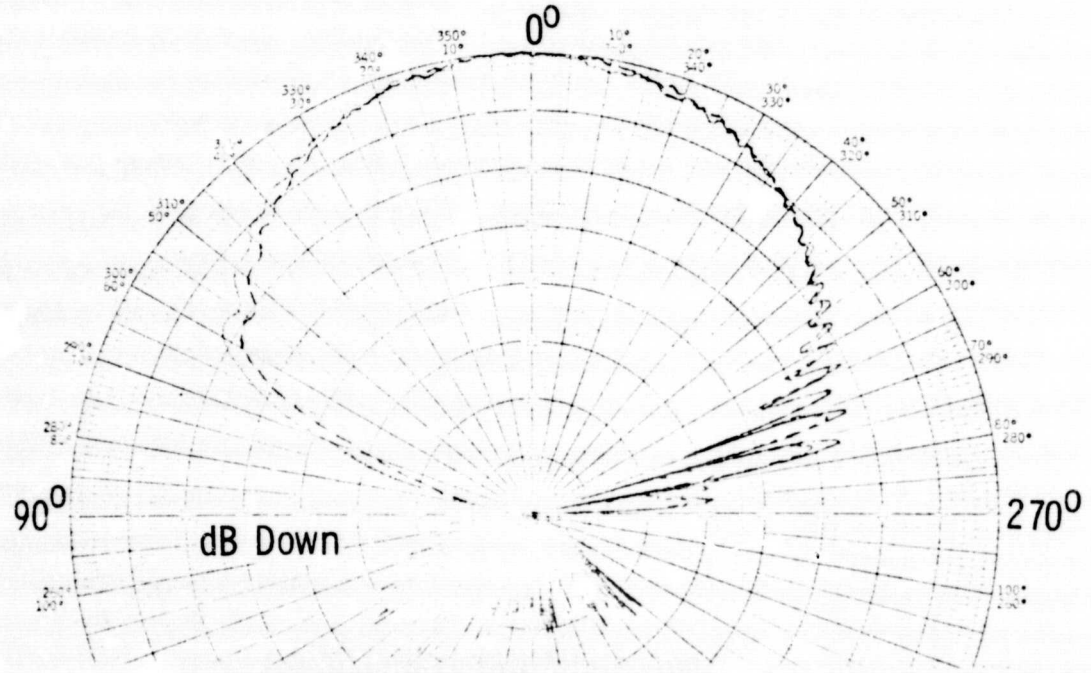

perpendicular polarization

d) d=19.05 cm

Fig. 4. Continued.

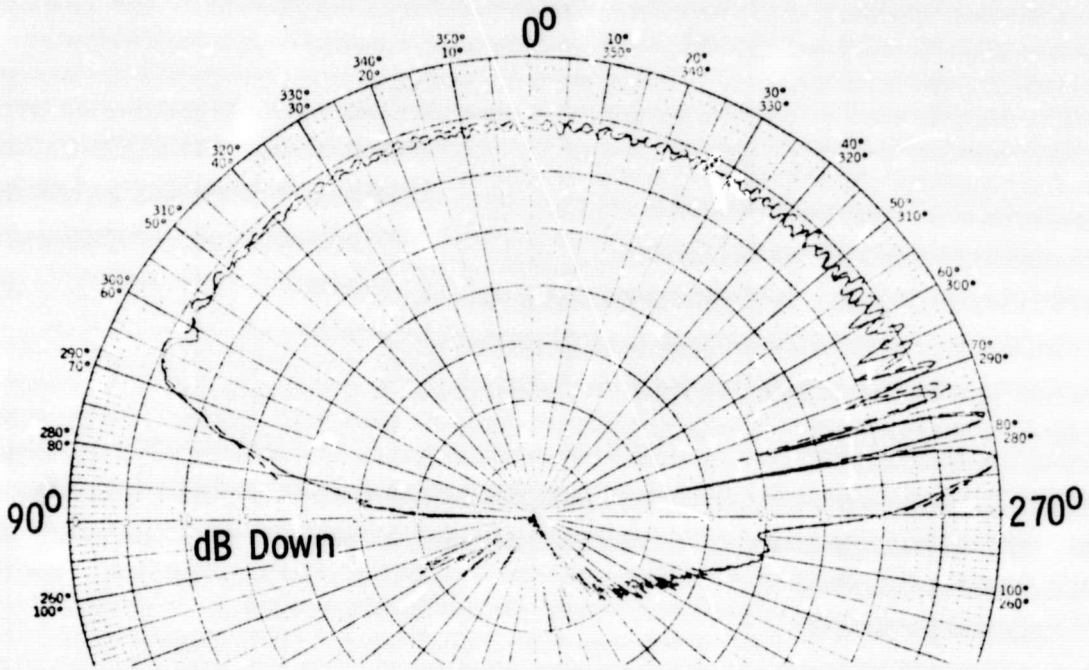

parallel polarization

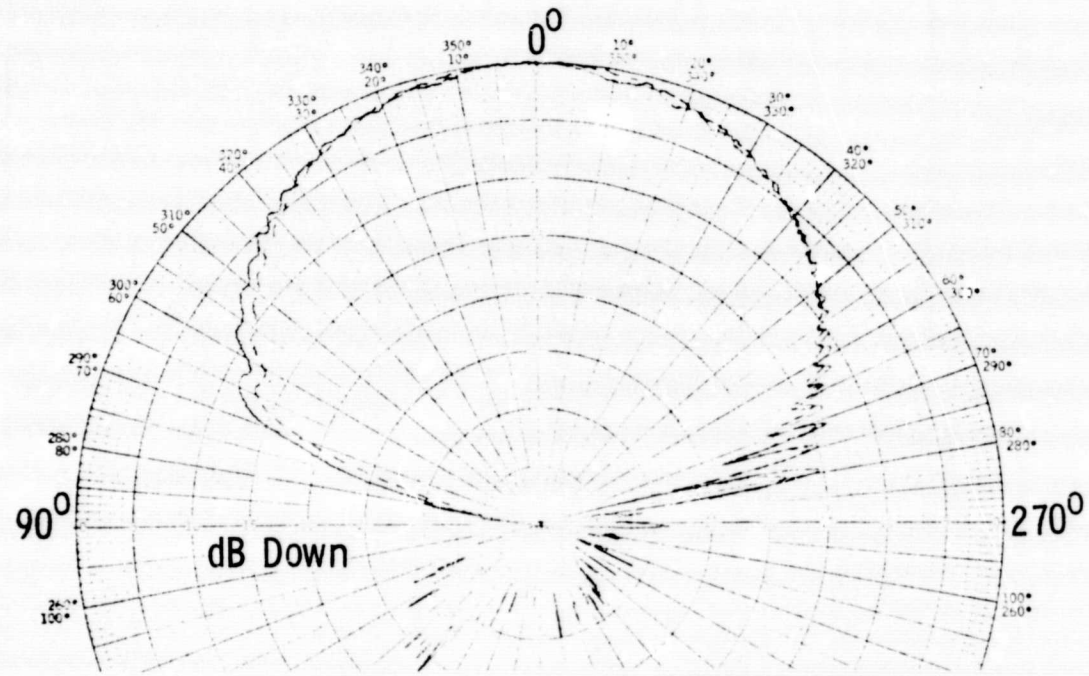

perpendicular polarization

e) d = 25.40 cm

Fig. 4. Concluded.

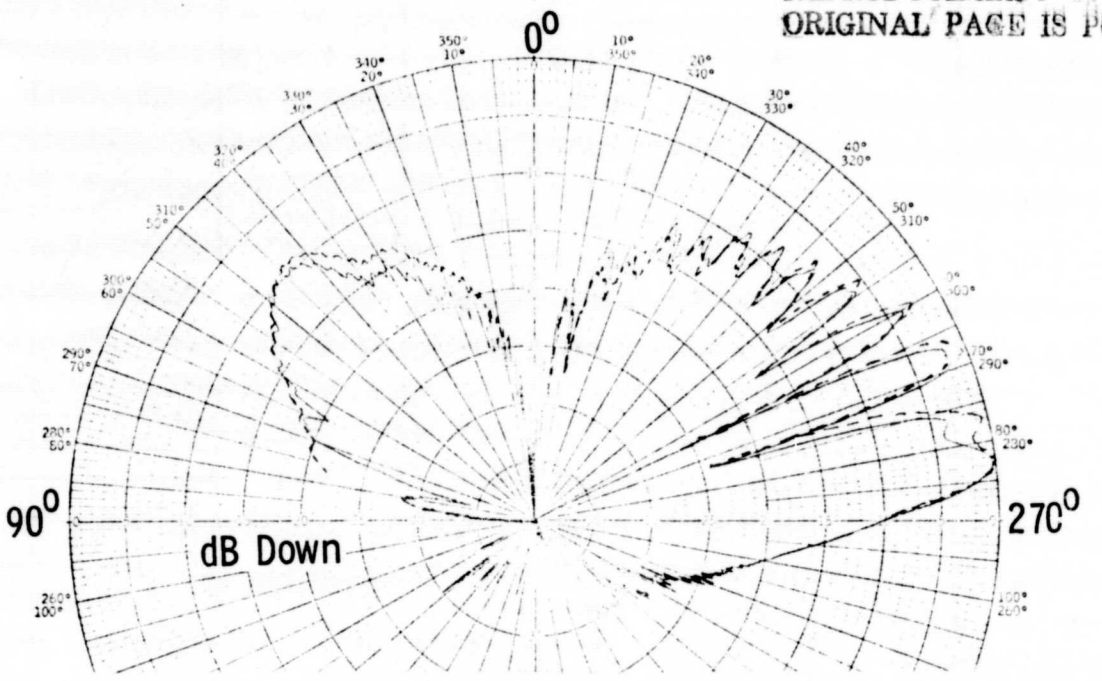

a) d=7.62 cm

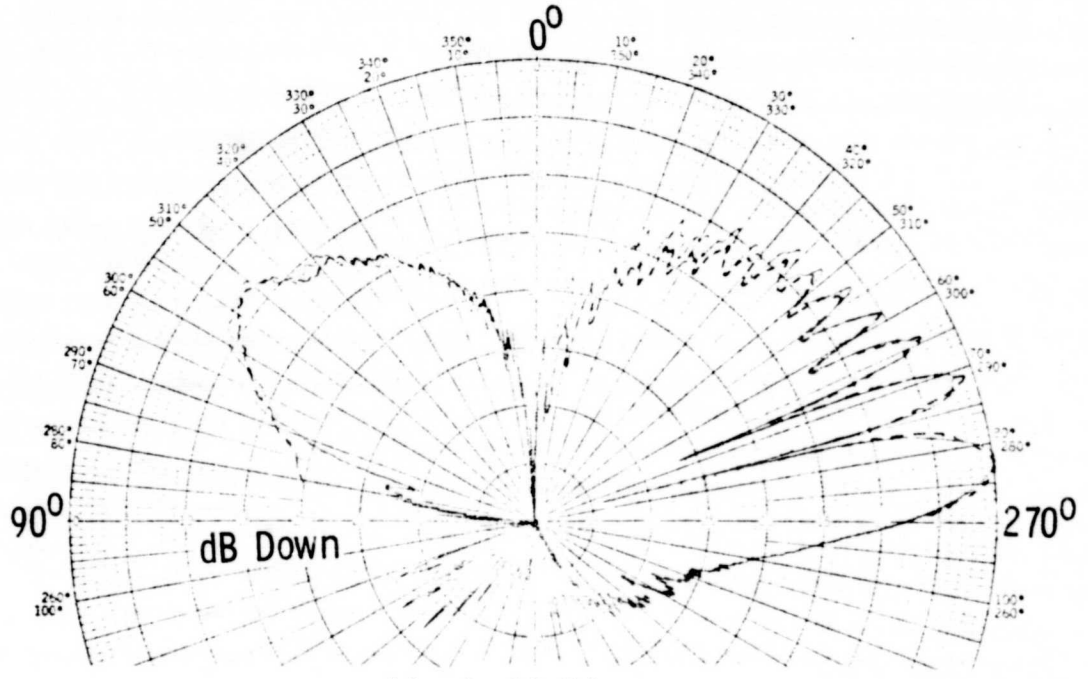

b) d=10.16 cm

Fig. 5. Elevation-plane patterns of $1/4\lambda$ electric monopole for h=5.08 cm at 35. GHz. Calculated– – –, Measured———.

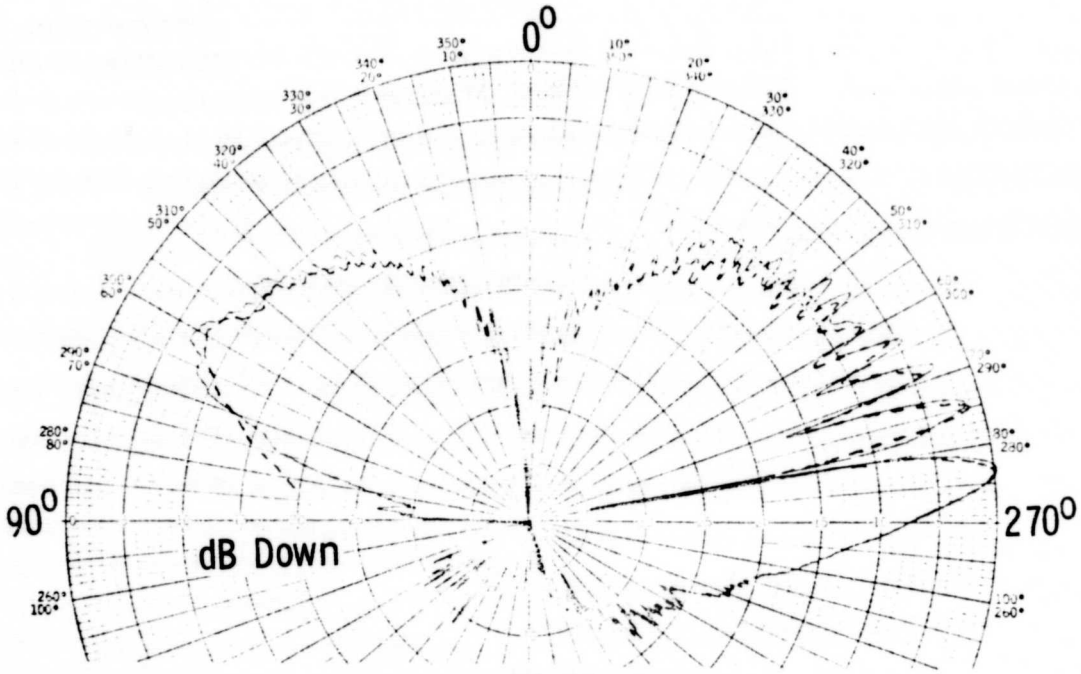

c) d=13.94 cm

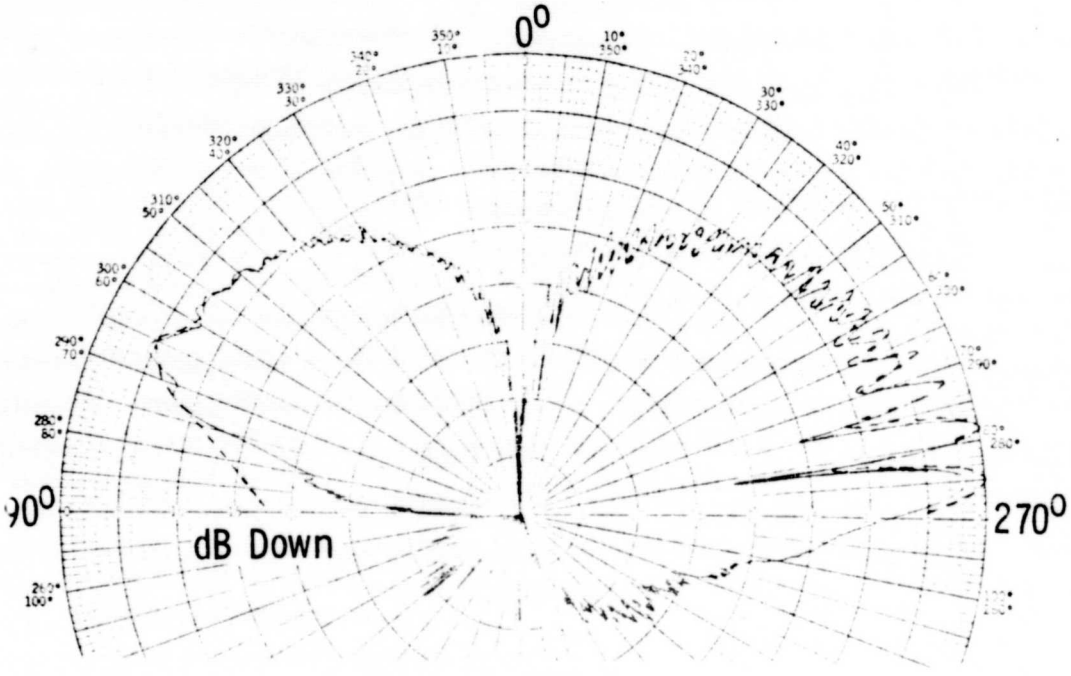

d) d=19.05 cm

Fig. 5. Continued.

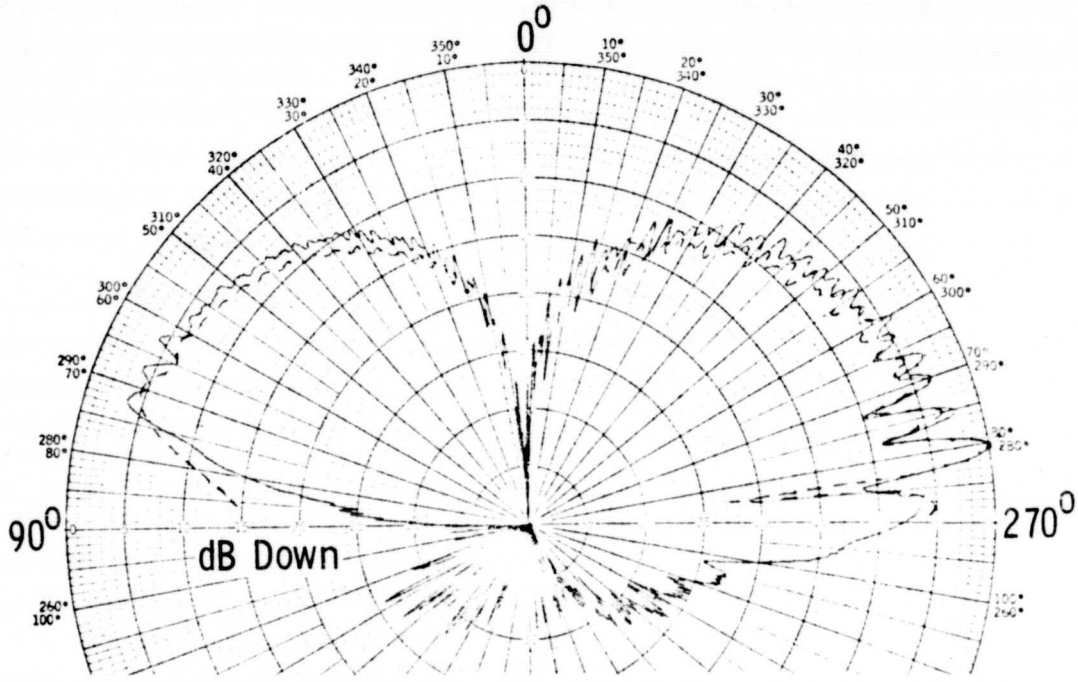

e) d = 25.40 cm

Fig. 5. Concluded.

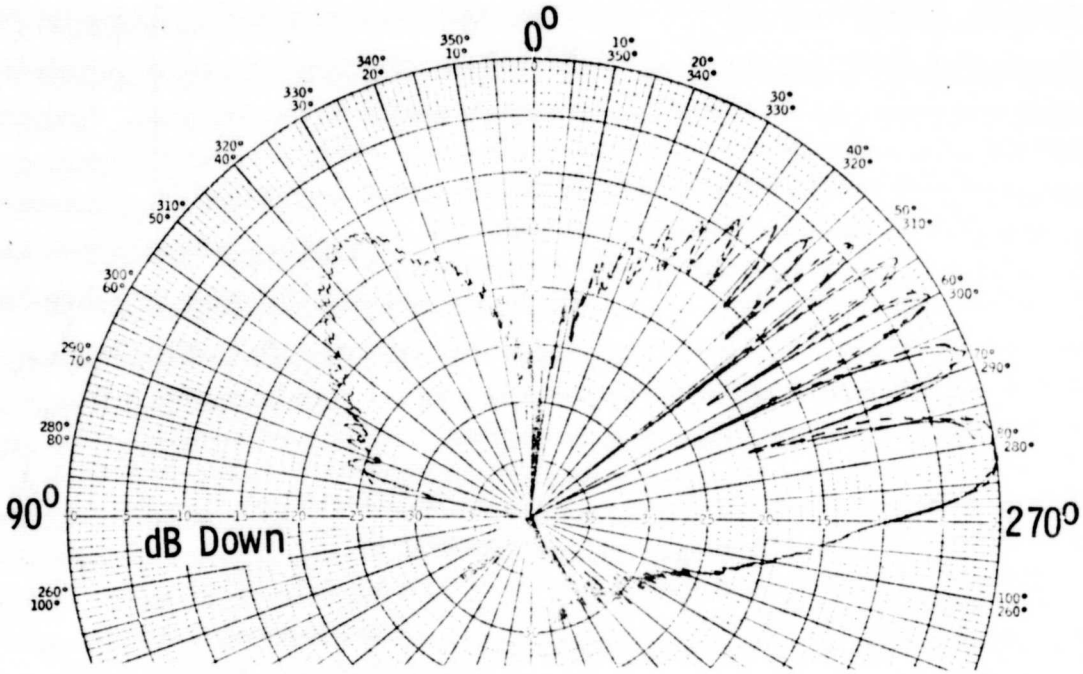

a) d=7.62 cm

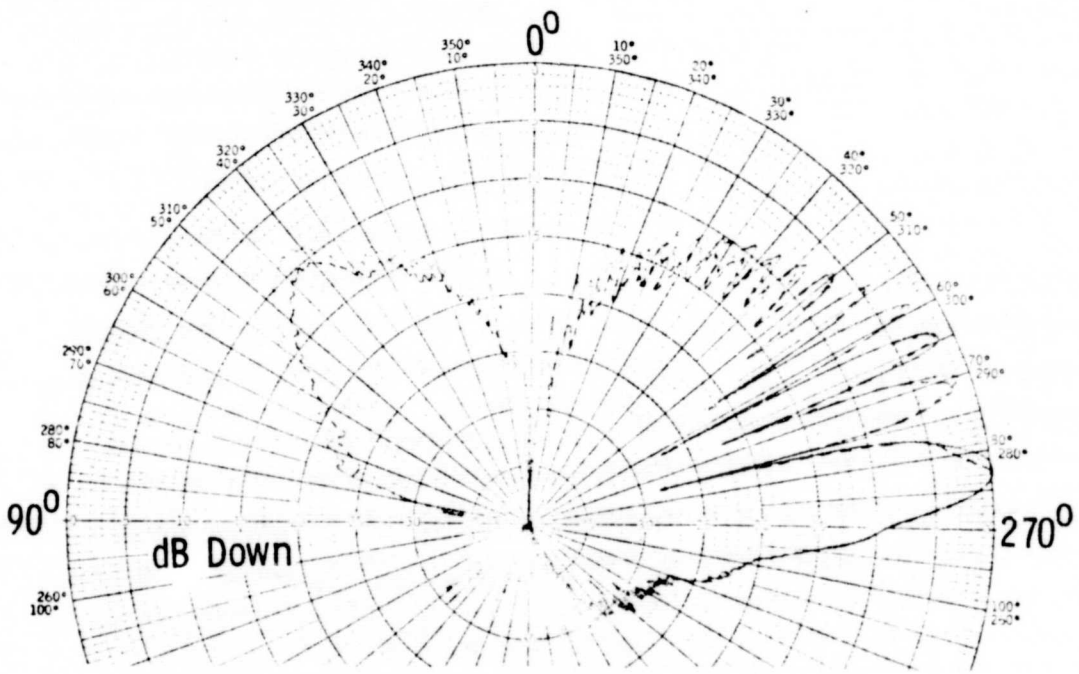

b) d=10.16 cm

Fig. 6. Elevation-plane patterns of $1/4\lambda$ electric monopole for h=7.62 cm at 35. GHz. Calculated - - -, Measured ——.

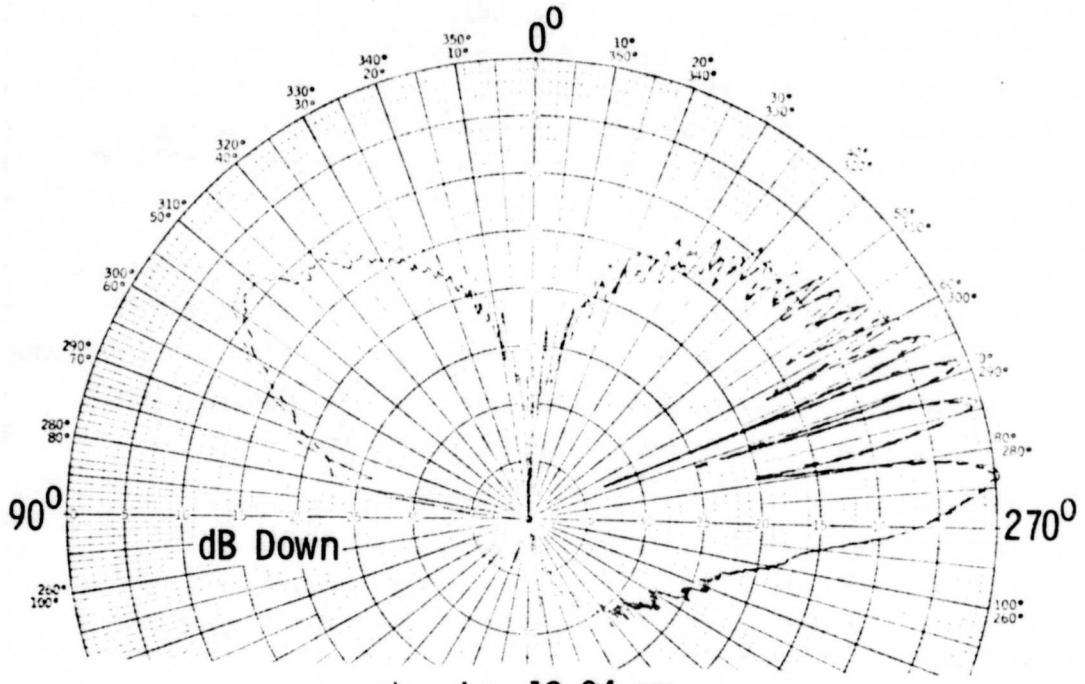

c) d = 13.94 cm

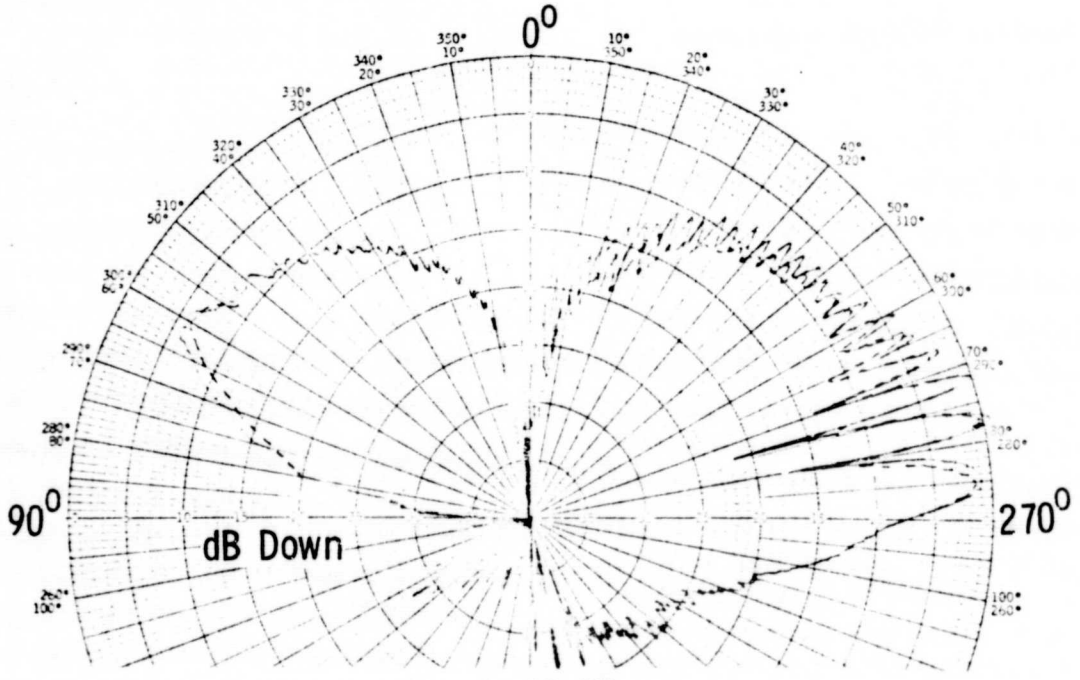

d) d=19.05 cm

Fig. 6. Continued.

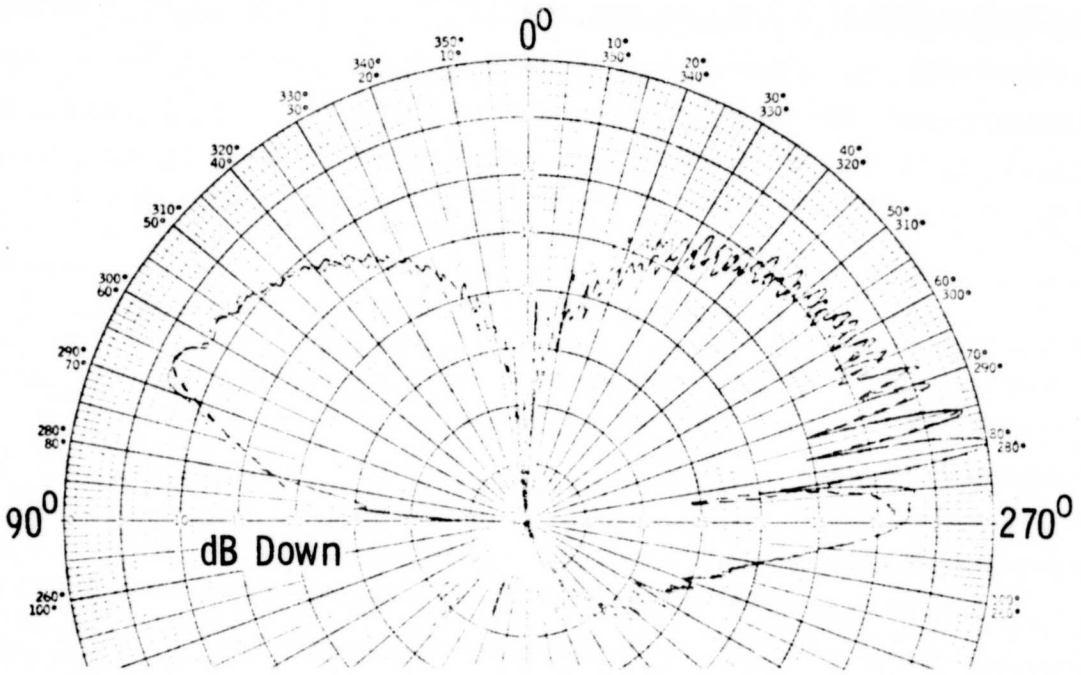

e) d = 25.40 cm

Fig. 6. Concluded.

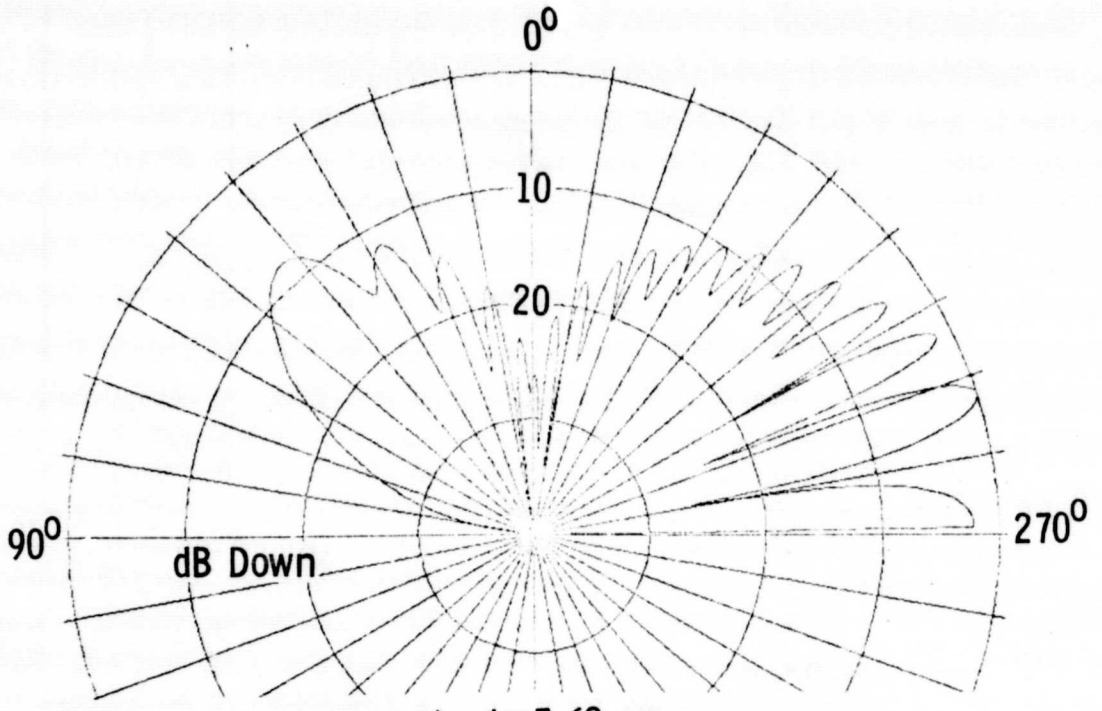

a) d=7.62 cm

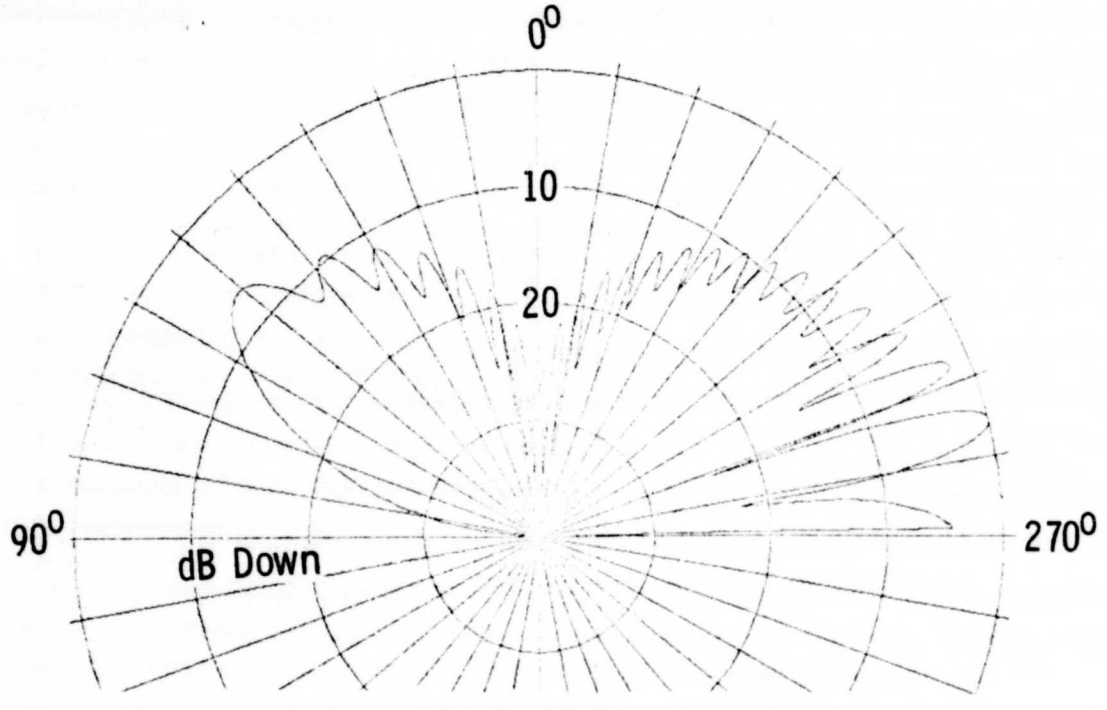

b) d=10.16 cm

Fig. 7. Calculated elevation-plane patterns of $1/4\lambda$ magnetic monopole for h=5.08 cm at 35. GHz.

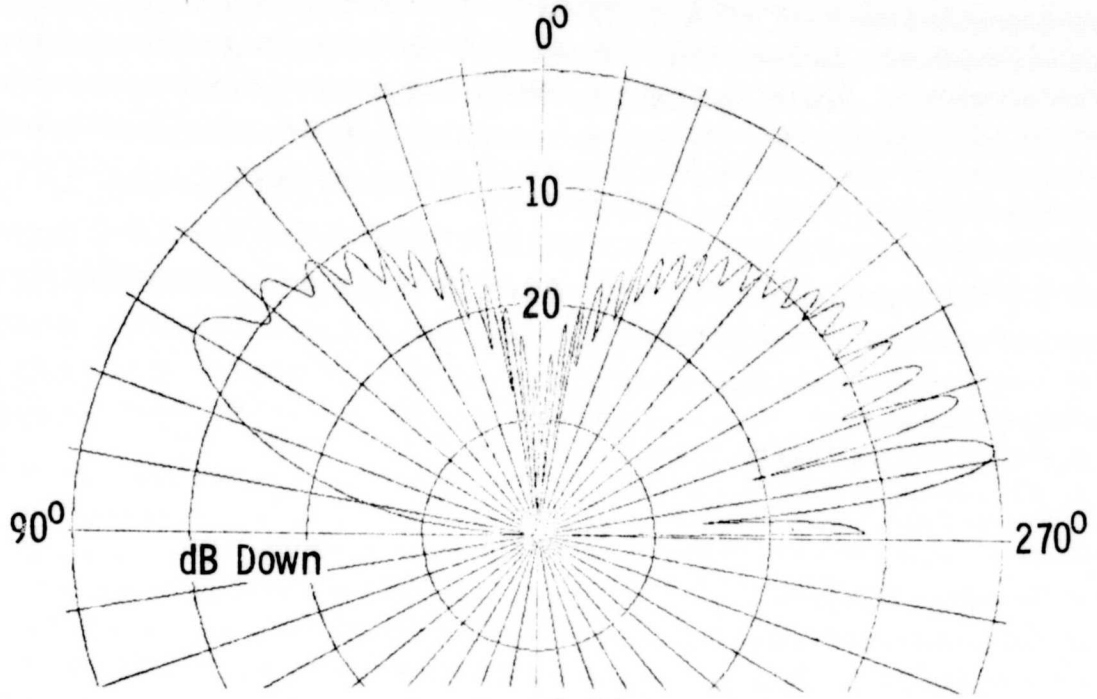

c) d = 13.94 cm

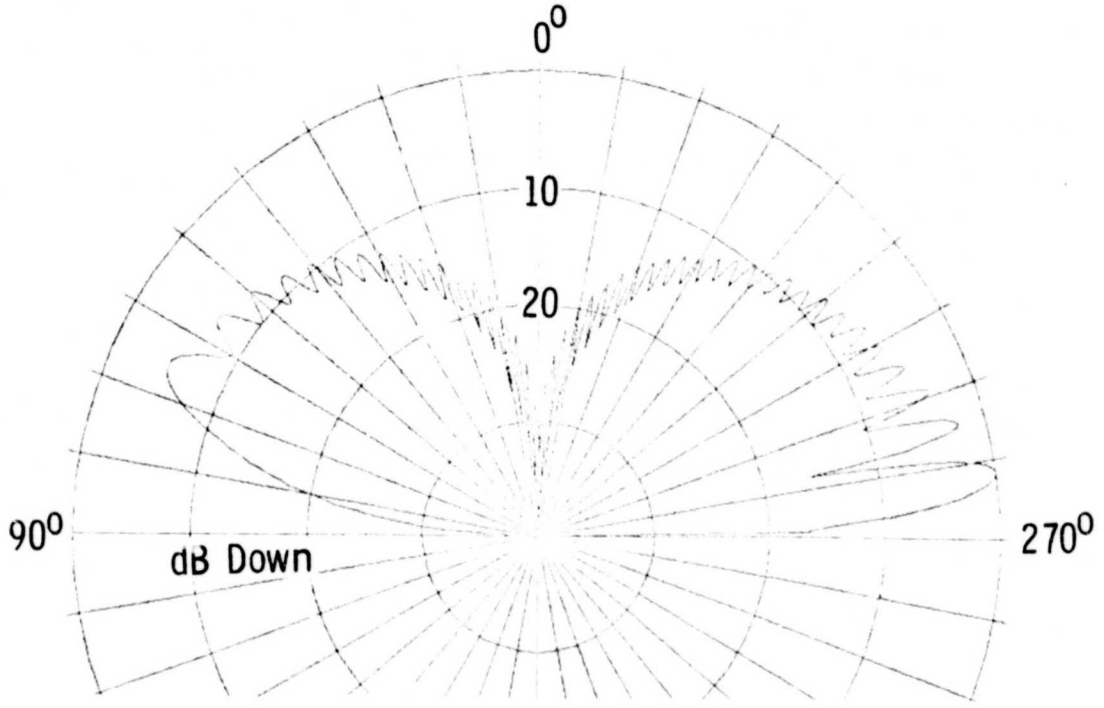

d) d = 19.05 cm

Fig. 7. Continued.

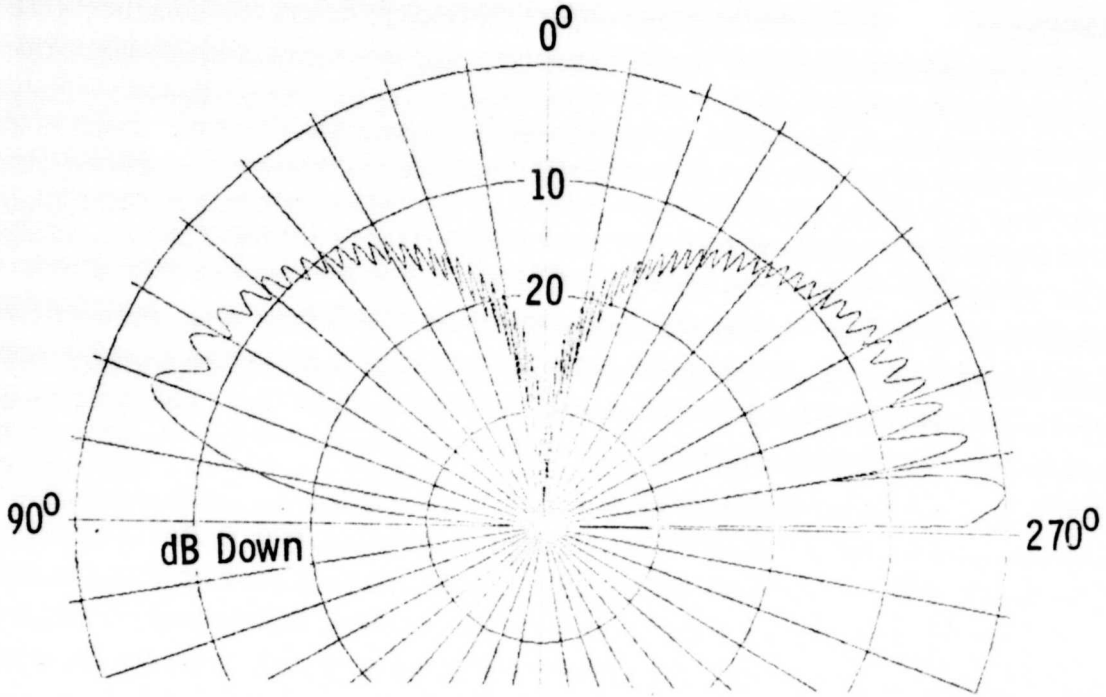

e) d= 25.40 cm

Fig. 7. Concluded.

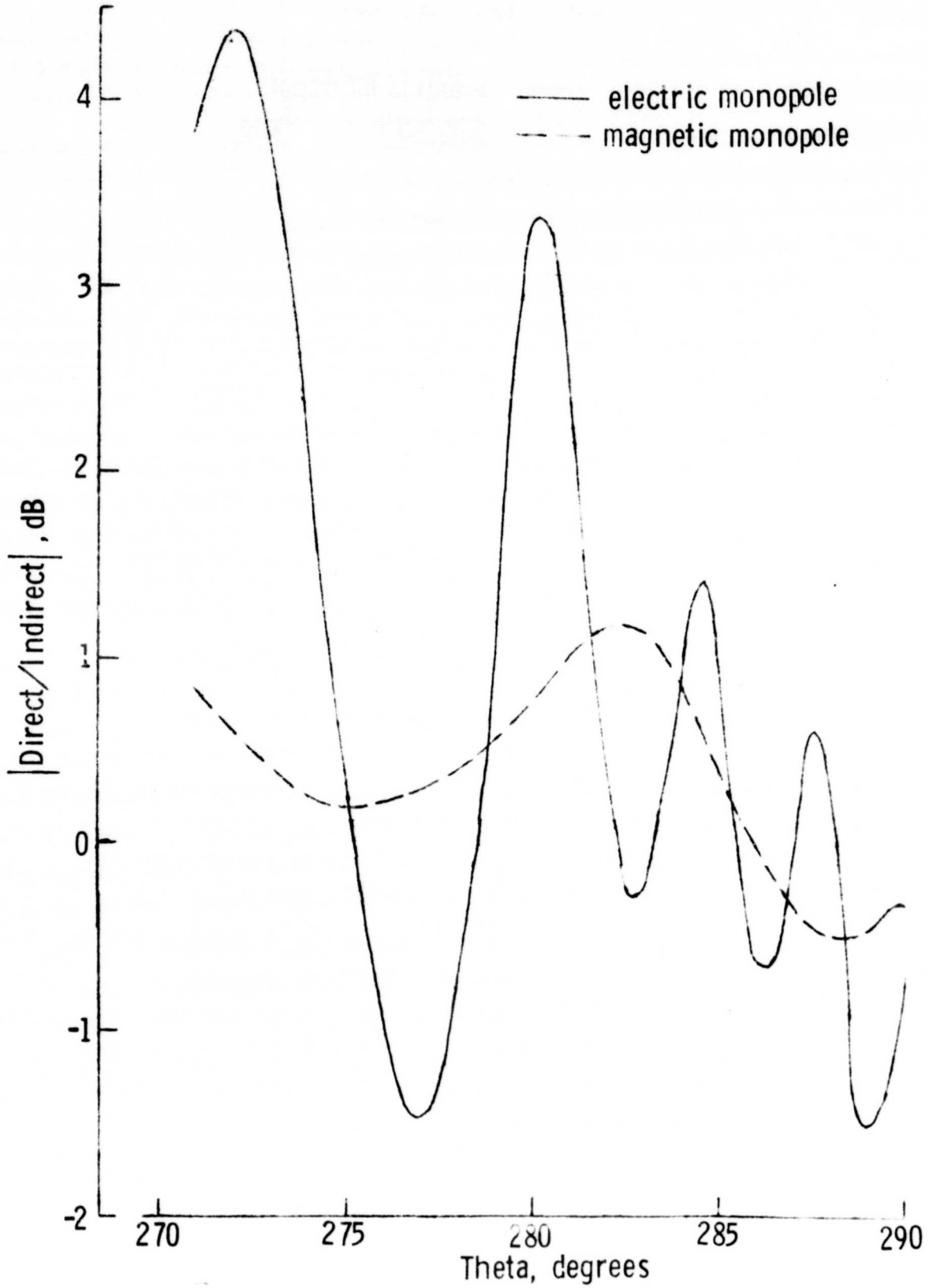

a) d = 7.62 cm

Fig. 8. Ratio of the magnitude of direct to indirect fields of monopoles as a function of elevation angle for h=5.08 cm.

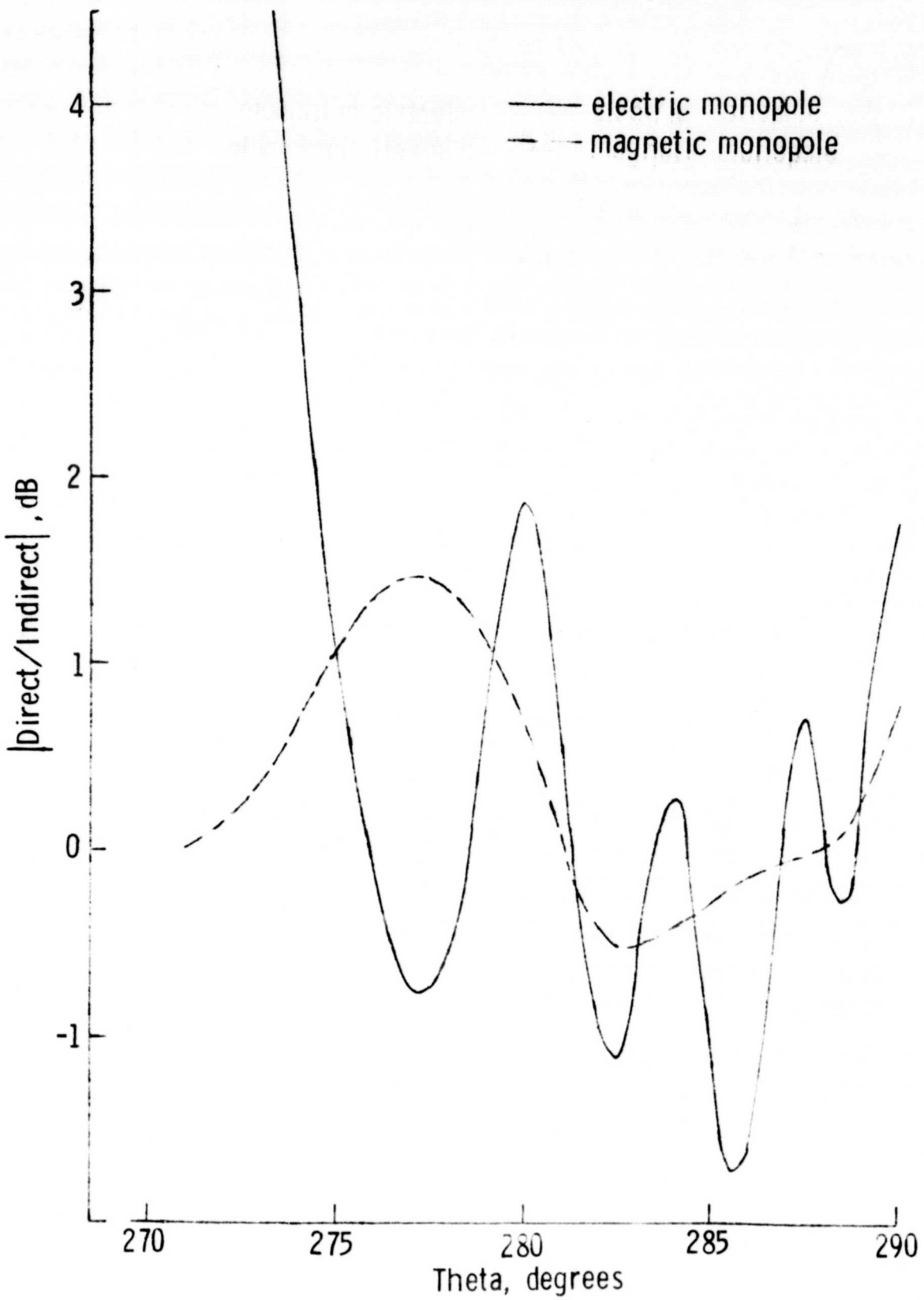

b) d=10.16 cm

Fig. 8. Continued.

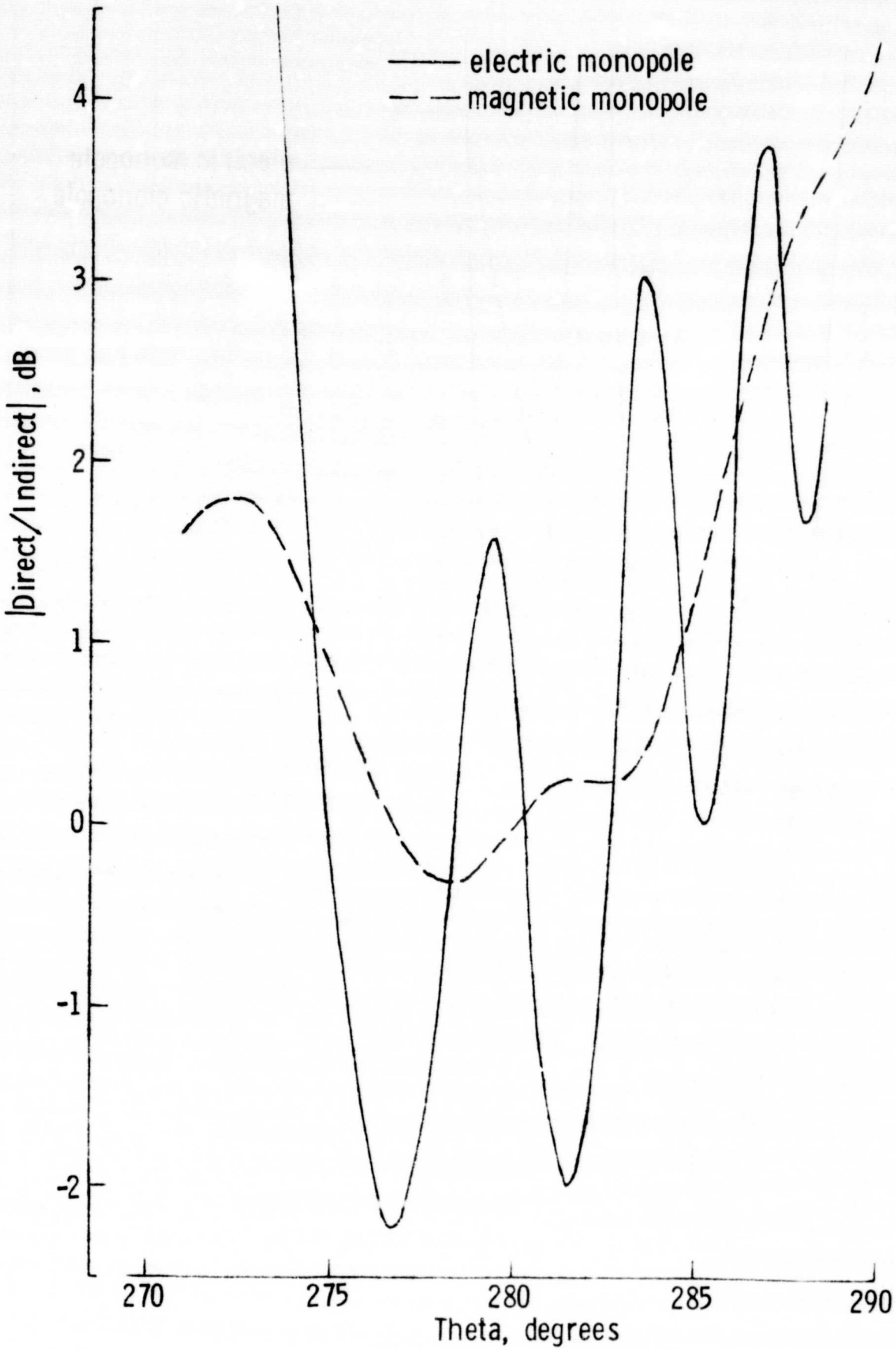

Fig. 8. Continued. c) d=13.94 cm

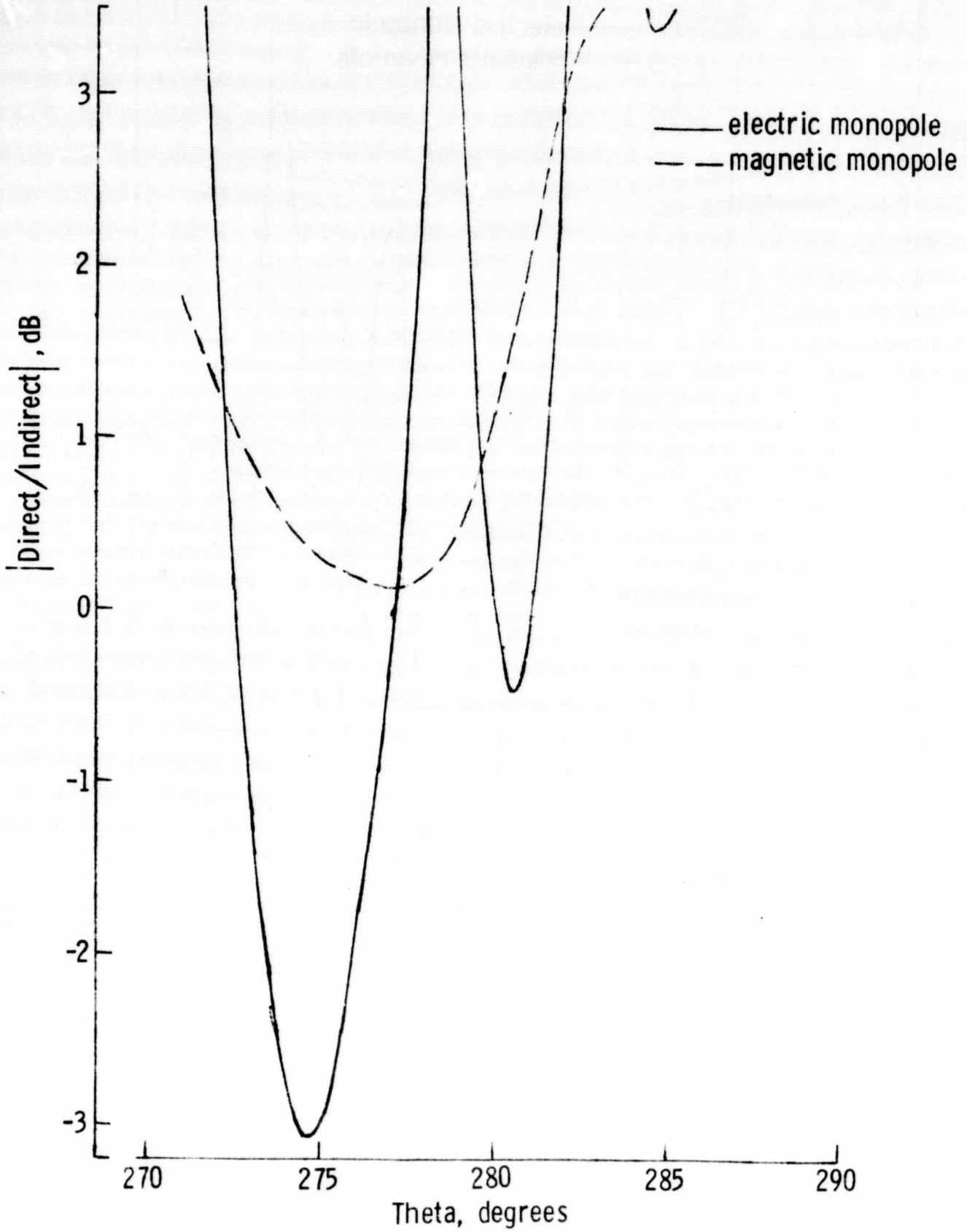

Fig. 8. Continued. d) d =19.05 cm

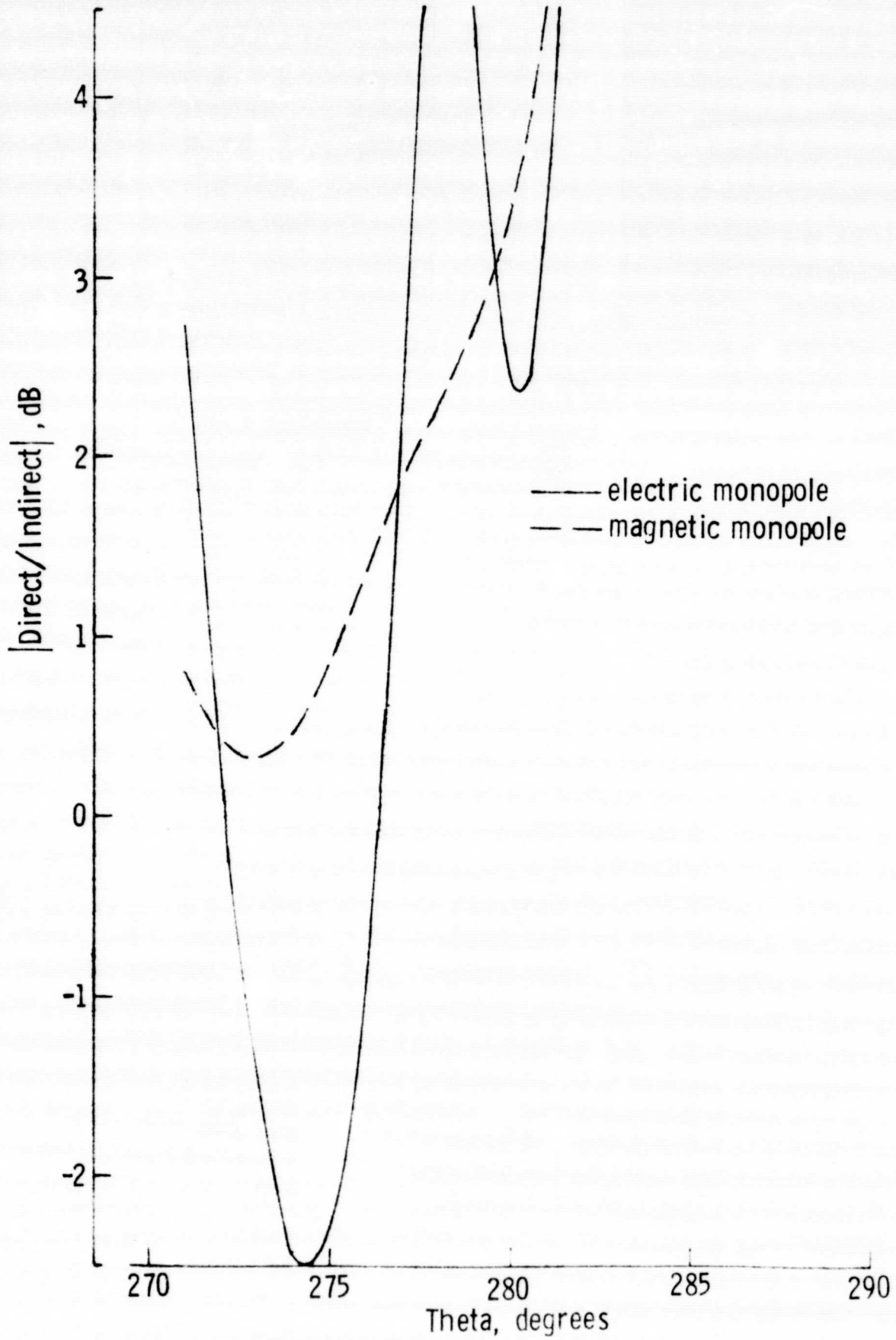

Fig. 8. Concluded. e) d = 25.40 cm